

RESEARCH ARTICLE

A Comparative Study of Mathematical Models for the Tropical Cyclone Intensity—Size Relation

Jie Sun¹, Ming Cai^{1*}, Guosheng Liu¹, and Da-Lin Zhang²

¹Department of Earth, Ocean, and Atmospheric Science, Florida State University, Tallahassee, FL, USA. ²Department of Atmospheric and Oceanic Science, University of Maryland, College Park, MD, USA.

*Address correspondence to: mcai@fsu.edu

Despite considerable progress in tropical cyclone (TC) research, our current understanding and prediction capabilities regarding the TC intensity-size relation remain limited. This study systematically analyzes the key characteristics and performance of different types of mathematical models for TC intensity size relations using the 6-hourly Tropical Cyclone Extended Best Track Dataset spanning 1988 to 2020. The models investigated include statistical, idealized (e.g., Rankine vortex), parametric, and theoretical models. In addition to directly comparing the solutions obtained from individual models to the observed TC records, we assess the models that can produce a unique finite-sized radial profile of surface winds for each TC record—a minimal requirement to ensure that the predicted radial profile of the surface winds would align with the observed profile. The results reveal that a sufficient condition to guarantee a unique radial profile of surface winds is that the associated model can be written as a radial invariant quantity, although it does not guarantee a finite-sized profile. Only the effective absolute angular momentum (eAAM) model, among all the models examined in this study, meets the minimum requirement. Furthermore, the solutions obtained from the eAAM model are well correlated with their observational counterparts (85 to 95%) with little systematic bias and small absolute mean errors that are very close to the observational resolution. The eAAM model's ability to capture the complex intensity-size relation of observed TCs, in combination with these desirable features, suggests its high potential for gaining a better understanding of the underlying physics governing the observed TC intensity-size relation.

Citation: Sun J, Cai M, Liu G, Zhang DL. A Comparative Study of Mathematical Models for the Tropical Cyclone Intensity—Size Relation. *Ocean-Land-Atmos. Res.* 2024;3:Article 0035. https://doi. org/10.34133/olar.0035

Submitted 18 August 2023 Accepted 6 December 2023 Published 5 January 2024

Copyright © 2024 Jie Sun et al. Exclusive licensee Southern Marine Science and Engineering Guangdong Laboratory (Zhuhai). No claim to original U.S. Government Works. Distributed under a Creative Commons Attribution License 4.0 (CC BY 4.0).

Introduction

Tropical cyclones (TCs) are very destructive storms that may result in severe loss of lives and properties, especially for intense TCs that are referred to as "typhoons" over the western North Pacific Ocean basin or "hurricanes" over the North Atlantic Ocean basin. In addition to the translation speed, TC intensity and size are the two key factors in determining TC damage potential [1] because they are closely related to the severity of TC swirling winds, precipitation, and storm surge. The TC intensity refers to the maximum 1-min sustained surface wind $(V_{\rm MAX})$, and the TC size is herein denoted by the maximum radial extent of gale-force surface wind (i.e., 17 m s⁻¹ wind denoted as V_{17} ; R_{17}). The TC intensity and intensification rate are closely related to the initial TC size, as shown by both observational and numerical modeling studies [2-8]. Although there have been continuing improvements in forecasting TC tracks, limited progress has been made in TC intensity forecasts [9,10]. Toward the goal of improving forecasts for TC intensity and size, this study investigates the strengths and weaknesses of previously published models for TC intensity-size relations. Since TC intensity and size are two key factors that manifest TC thermodynamic and dynamic processes, improving the understanding of the TC intensity-size relation will help us gain insight into the core development mechanisms and the genesis of TCs.

Numerous studies have been carried out to represent or improve the TC intensity-size relationship, including the radial profiles of TC surface winds. In addition to numerical modeling studies, the models for the radial profiles of TC surface winds or the TC intensity-size relationship can be categorized into the following four types: (a) statistical models, (b) idealized models, (c) parametric models, and (d) principle-based models. Statistical models are based on linear regression between the observed TC intensity and size, which can be used to estimate TC intensity from size information or TC size from intensity information [11-14]. Some statistical models also consider environmental parameters, such as sea-surface temperature, synoptic flows, and track types [5,8,15-18]. However, the observed TC intensity and size exhibit a weak correlation, which also varies greatly when different datasets are used [11,19]. Even with most up-to-date observation data and higher-order nonlinear regression functions, recent studies still indicate weak correlations between TC intensity and size [8,20–23]. Recently, Guo and Tan [6] introduced a size-related compound parameter, referred to as "TC fullness." The TC fullness is proportional to the annulus area encircled between the radii of $V_{\rm MAX}$ and $V_{\rm 17}$. The TC intensity is better correlated with its size after sorting TC records by their fullness. The studies of Wu and Ruan [24] and Ruan and Wu [25] have confirmed the higher correlation after segregating TC records according to the radii of V_{MAX} .

Studies on TC wind profiles can be traced back to the use of the Rankine [26] vortex model by Deppermann [27], which essentially treats the relative angular momentum of a TC as a radial invariant quantity. Since then, various versions of Rankine vortex models have been proposed by considering a nonlinear dependency of the relative angular momentum on radii [28–31]. A widely used idealized model for radial profiles of TC surface winds was proposed by Holland [32] (H80 hereafter) and later revised by Holland et al. [33] (H10 hereafter) under the assumption of cyclostrophic balance of TC surface wind, instead of a simple radial invariance of the relative angular momentum. Because of the use of cyclostrophic balance, as demonstrated by Zhang et al. [34], the H10 model represents a noticeable improvement over the other versions of Rankine vortex models in characterizing the radial variation in surface winds in the inner core region of TCs. However, the H10 model is not valid in the large-sized outer region of TCs because it neglects the planetary angular momentum.

Parametric models describe the radial profile of TC surface winds as a function of its distance from the storm center. Observational evidence suggests that the rotational wind within the TC vortex core behaves like a solid-body rotation [28,35–38]. Parametric models assume a circular wind flow pattern in the surface layer and usually use a few (2 to 5) parameters to fit "typical" radial profiles of observed TCs [36,37,39]. Wang et al. [40] proposed a single-parameter wind profile model, which shows a good fitting skill against TC wind profiles simulated by numerical models. Some parametric models, such as the piecewise multiparameter model by Wood and White [39], can partition the wind profile into separate components according to the actual numbers of maximum wind cusps in the wind profile to better match the realistic observations of single-, dual-, and triple-concentric eyewall complex vortex structures. The parameters in these models can typically be adjusted to individual observed or simulated TC profiles for a wide range of applications, such as hurricane risk modeling or initializing wind fields for numerical models. Parametric models are often used to construct initial wind profiles for numerical TC simulations [41], storm surge modeling [42], and tornado modeling [43,44].

The seminal work by Emanuel [45] was the first theoretical study to introduce the Carnot engine model for TC intensity. Emanuel [46] (E04 hereafter) developed a theoretical formula for the radial derivative of the absolute angular momentum (AAM) of TC surface winds, which can be used to construct the radial profile of TC surface winds. An analytical solution from the Carnot engine model was later derived by Emanuel and Rotunno [47] (hereafter ER11), in which the AAM at any radius in the boundary layer of the inner convective core region is related to the radial loss of enthalpy and momentum. The analytical solution reported in the ER11 model also serves as a model for the radial profile of TC surface winds. By recognizing that the E04 model focuses more on the outer region of TC, whereas the ER11 model focuses more on the inner core region where kinetic energy is generated, Chavas et al. [48] (C15 hereafter) merged the ER11 model for the inner region with the E04 model for the outer region as a single model for the entire radial profile of TC surface winds. Recently, Cronin [49] provided an alternative approach to obtaining the entire wind profile as in C15 but with much less computational effort. Specifically, he derived an analytical function of the E04 model's wind speed as a function of radius, which is then merged with

the inner region solution represented by ER11. Note that this analytical solution can also be used to directly estimate the radius (R₀), where TC wind vanishes, using the maximum wind information without obtaining the entire wind profile. Inspired by the work of ER11, E04, and C15, Sun et al. [50] (S22 hereafter) recently put forward an effective AAM (eAAM) model, which combines the AAM and the loss of both the relative angular momentum and planetary angular momentum due to surface drags as a radial invariant quantity, instead of the relative angular momentum or AAM itself. In the eAAM model, the AAM of an air parcel in the surface layer, as it flows cyclonically from the outer region to the radius of the maximum sustainable wind, decreases inwardly because of surface drag. Note that the radial invariant of eAAM in the eAAM model would be reduced to the radial invariant of AAM when the coefficients for the loss terms are set to zero, which is not the case in the E04, ER11, and C15 models. The advantage of considering a radial invariant quantity is its potential to have the quality of physical laws when calculating the TC intensitysize relationship.

Considering the growing interest in the TC intensity–size relationship and its importance in assisting operational assessment of TC severity and potential damage, we systematically examine the performance skill of each model type for TC intensity-size relation against observations and compare them to that of the eAAM model using the 6-hourly Tropical Cyclone Extended Best Track Dataset (EBTRK) [51]. The rest of the paper is organized as follows. The next section describes the data and the metrics used for this study to quantify the performance skill of the four different types of models. In the "Performance evaluations" section, the performance evaluations are compared against the observations of all models analyzed in this study. The "Mathematical characteristics for enabling a better physical understanding" section discusses the mathematical characteristics of these models in terms of their feasibility for gaining a physical understanding of the observed TC intensity–size relation. A summary and concluding remarks are given in the final section. In Appendix A, we outline the procedures for obtaining the solutions to the models.

Materials and Methods

The variables used in this study are derived from the 6-hourly EBTRK covering TC records from 1988 to 2020 over the North Atlantic Ocean region, which is downloaded from https:// rammb2.cira.colostate.edu/research/tropical-cyclones/tc_ extended_best_track_dataset/. They include the maximum (sustained) surface wind speed ($V_{\rm MAX}$), which represents TC intensity, the radius of maximum wind speed (R_{MAX}), and the radius of gale force wind (R_{17}) , which represents TC size, in addition to latitude and longitude information of each corresponding TC record. The speed of the gale force wind is equal to 34 knots or 17.5 m s⁻¹, which is denoted as V_{17} . Following Guo and Tan [6], we consider the average of the four values of R_{17} as the TC size, although in many other studies [52], the largest R_{17} value in the four quadrants is used as R_{17} after multiplying a correction factor (0.85 in [52]). According to the EBTRK dataset, the resolution of maximum TC surface winds is 10 knots (approximately 5.2 m s⁻¹), and the resolution of radii (both R_{MAX} and R_{17}) is 5 n mi (approximately 9.3 km).

The EBTRK dataset from 1988 to 2020 has a total number of 12,235 TC records. We only consider 4,984 of them that meet

the following conditions for the purpose of our study: (a) containing both $V_{\rm MAX}$ and $R_{\rm MAX}$, with at least three quadrants of R_{17} available; (b) $R_{\rm MAX} < R_{17}$; (c) at least the strength of tropical storms; (d) TC over the ocean region (distance to the nearest land point is greater than R_{17}); and (e) $({\rm AAM})_{\rm MAX}$ (i.e., AAM at $R_{\rm MAX}$) smaller than $({\rm AAM})_{17}$ (i.e., AAM at R_{17}). Notably, condition (e) is necessary for the existence of the solutions to the E04, ER11, C15, and eAAM models. Note that the TC records that do not meet condition (e) cover less than 5% of the total TC records. In terms of TC intensity, the 4,984 TC records used in this study consist of 2,360 tropical storms and 1,438 category 1,522 category 2, 328 category 3, 299 category 4, and 37 category 5 cases of hurricanes. Notably, the calculation of the distance to the nearest land in the EBTRK data omits islands with an area smaller than that of the island of Trinidad (approximately 4,800 km²).

There are two types of considerations for evaluating the performance skill of individual models regarding the observed TC records. The first is a set of quantitative metrics that facilitate direct comparison between the solutions obtained from individual models and the observed TC records. These metrics are listed in Table 1. The "Performance evaluations" section focuses on the performance evaluations using the metrics listed in Table 1. The second type of consideration is a list of mathematical characteristics that are deemed necessary to gain a better understanding of the underlying physics governing the observed TC intensity—size relation, which will be discussed in the "Mathematical characteristics for enabling a better physical understanding" section. These mathematical characteristics that allow for gaining a better physical understanding include

- a. The uniqueness of profiles for winds and radii: Both the profile of surface winds as a function of R [i.e., V(R)] and the profile of radii as a function of surface winds [i.e., R(V)] exist, where R(V) is the same as the inverse function of V(R), and vice versa.
- b. Finite-sized TC profiles: Surface winds vanish at finite values of $R_0 = R(V = 0)$ and $V(R = R_0) = 0$.
- Similarity: The probability density function of the intensity size relation obtained from a model should resemble that observed.

We recognize that the models being assessed are not inherently tailored to optimize performance on the metrics. Our focus on these metrics is intended to assess the individual models' capacity for gaining a better physical understanding, rather than merely for their numerical accuracy. For example, models that possess characteristics (a) are expected to generate unique solutions. Because of the uniqueness, the condition that the solution is accurate against the radial profile of an observed TC at a given radius would automatically ensure that the solutions are equally accurate over the entire radial profile. Unless meeting the uniqueness condition, achieving good skill in both predicting TC intensity using size information and predicting TC size using intensity information by the same model would not be feasible. Thus, models that do not meet the uniqueness condition would have limited potential to gain a better physical understanding of the TC intensity-size relation. The radius of zero azimuthal wind, while challenging to precisely identify through observations, is considered a theoretical limit for TC winds. This limit exists in numerical models for isolated TCs, such as the cloud model 1 by Bryan and Fritsch [53]. Consequently, it is an essential feature that provides an upper bound for the outermost radius of azimuthal winds in the range of 5 to 10 m s⁻¹. Therefore, models that possess characteristics (b) would have the potential to improve our understanding of the outskirt wind structure and its link to the inner core wind structures. Models that fulfill characteristics (a) to (c) can be considered to have met the minimum necessary conditions to demonstrate the quality of physical laws, because such models are expected to produce solutions that agree with observations within the range of observational resolution, regardless of whether wind or radius is used as an input variable.

It is worth mentioning that a secondary eyewall is typically associated with high-intensity TCs, while none of the analytical models examined in this study have the capability to make its prediction. Moreover, since there is no information in the EBTRK dataset about TC asymmetry and the secondary maximum wind speed, two implicit assumptions must be made for TC wind for our examination, i.e., axisymmetric and monotonically decreasing outward. Accordingly, all following results are based on these assumptions without considering a secondary

Table 1. A list of metrics for the direct comparison against observations

Names	Definition
Mean absolute errors (MAE)	$MAE = \overline{ X_{solution} - X_{obs} }^{a}$
Correlation (Corr)	$Corr = \frac{\frac{(\chi_{\text{solution}} - \overline{\chi}_{\text{solution}})(\chi_{\text{obs}} - \overline{\chi}_{\text{obs}})}{\sqrt{(\chi_{\text{solution}} - \overline{\chi}_{\text{solution}})^2}} \sqrt{(\chi_{\text{obs}} - \overline{\chi}_{\text{obs}})^2} a$
Mean errors (MErr)	$MErr = \overline{X}_{solution} - \overline{X}_{obs}^{ a}$
Number of unphysical solutions	Number of unphysical solutions b

^aThe overbar is the averaging operator over all TC records; X can be any of the four variables: V_{MAX} (maximum wind speed), R_{MAX} (radius of maximum wind speed), V_{17} (gale-force wind speed), and R_{17} (radius of gale-force wind speed).

^b For V_{MAX} , unphysical solutions include no real number solutions, and $V_{\text{MAX}} < (V_{17})_{\text{obs}}$; for V_{17} , unphysical solutions include no real number solutions, $V_{17} < 0$, and $V_{17} > (V_{\text{MAX}})_{\text{obs}}$; for R_{MAX} , unphysical solutions include no real number solutions, $R_{\text{MAX}} < 0$, and $R_{\text{MAX}} > (R_{17})_{\text{obs}}$; for R_{17} , unphysical solutions include no real number solutions, and $R_{17} < (R_{\text{MAX}})_{\text{obs}}$.

eyewall. Therefore, the models that possess characteristics (a) to (c) may not be comparable to the TC records for asymmetric TCs with/without secondary wind maxima. Nevertheless, models meeting the uniqueness condition would still yield an overall better skill than models that do not meet these conditions.

Performance Evaluations

In this section, we systematically evaluate the performance of representative models from each of the four categories (i.e., statistic, idealized, parametric, and physical-based models) and the eAAM model against observations using the metrics listed in Table 1.

Statistical models

All statistical models suffer a major deficiency, namely, they can be used to estimate either the intensity from size information or the size from intensity information, but not the other way around without significant changes in model parameters. As a result, they provide little insight into the observed TC intensity-size relationship, even though the correlation skill can be improved by considering nonlinearity and compound parameters that are related to intensity, size, track types, and/ or environmental variables. Therefore, we evaluate only one of them to illustrate the performance skill and the general characteristics of statistical models. That is, the statistical model reported by Wu et al. [20] (W15 hereafter) is evaluated herein, which was built from a nonlinear regression analysis of R_{17} and $V_{
m MAX}$ using the Multiplatform Tropical Cyclone Surface Wind Analysis dataset (MTCSWA) [54]. Specifically, the W15 model is given by

$$R_{17} = -1.23 + 0.07V_{\text{MAX}} - 0.0004V_{\text{MAX}}^2 \tag{1}$$

Although the W15 model, by design, is for estimating the size (i.e., R_{17}) using the intensity information (i.e., $V_{\rm MAX}$), we still attempt to obtain $V_{\rm MAX}$ from R_{17} and R_{17} from $V_{\rm MAX}$. We also note that the W15 model was built using TC records over the western North Pacific, while here, we attempt to apply the W15 model to TC records over the North Atlantic basin. As to be demonstrated shortly, the error magnitude of the W15 model for R_{17} verified against the TC records over the North Atlantic basin is comparable to that verified against TC records over the western North Pacific.

The scatterplots of W15's solutions versus observations for $V_{\rm MAX}$ and R_{17} are displayed in Figs. 1A and 2A, respectively. Figure 3 shows the W15 values of the four metrics listed in Table 1. The small positive correlation of the W15 solutions for $V_{\rm MAX}$ with the observed $V_{\rm MAX}$ (approximately 0.32; Fig. 3A) is expected, as the W15 model is designed only for estimating R_{17} using observed $V_{\rm MAX}$. However, it is surprising to find that the W15 solutions for R_{17} also fail to produce a good correlation with the observed R_{17} (Fig. 2A), despite being built on the regression analysis of the observed $V_{\rm MAX}$ and R_{17} . In fact, the correlation between the W15 solutions for R_{17} and the observed R_{17} is even weaker (approximately 0.28; Fig. 3B) than that for $V_{\rm MAX}$. This is direct evidence for the lack of correlation between $V_{
m MAX}$ and $R_{
m 17}$ in the observations. The relatively good performance of W15's solutions for $V_{\rm MAX}$ over that for R_{17} , in terms of MAE, Corr, and MErr, is achieved at the expense of the fact that nearly 63% of the W15 solutions for $V_{\rm MAX}$ are unphysical (i.e., either no real number solutions, which are not shown in Fig. 1A, or solutions for $V_{\rm MAX} < V_{17}$, which are marked by red circles in Fig. 1A), since these unphysical solutions are not used to calculate the metrics of MAE, Corr, and MErr. The results shown in Fig. 3A indicate that the error magnitude of the W15 model for R_{17} verified against the TC records over the North Atlantic basin (approximately 70 km) is comparable to that verified against TC records over the western North Pacific (approximately 95 km, as shown in figure 2 of W15).

Because the W15 model does not involve variables beyond $V_{\rm MAX}$ and R_{17} , it is not applicable to evaluate the performance metrics for its V_{17} and $R_{\rm MAX}$ or to provide information related to the general characteristics (a) to (c) discussed in Materials and Methods. Although other statistical models very likely have different error characteristics, the W15 model can still be regarded as being representative in terms of its inability to possess general characteristics (a) to (c). Specifically, all the statistical TC intensity-size models relate a TC parameter on the left-hand side of the model equation, either intensity or size, to the other TC parameters on the right-hand side. Therefore, the statistical models are excluded from possessing these three characteristics by design, even if they would have a very high skill for predicting the TC parameter on the left-hand side. As a result, statistical models provide little physical insight into the observed TC intensity–size relationship.

Idealized models

The Rankine vortex model [26] first used by Deppermann [27] is the first idealized model for radial profiles of TC surface winds, in which the relative angular momentum of a TC is a radial invariant quantity. Since then, various versions of Rankine vortex models have been proposed by including a nonlinear radial dependency of the relative angular momentum [28,30,31]. More widely used idealized models for radial profiles of TC surface winds are the H80 and H10 models. For the sake of completeness, we evaluate the original Rankine vortex model (denoted as the "RANK" model), a modified Rankine vortex model first used by Riehl [28] (denoted as the "MRank" model), and the H80 model, whose equations are given by

$$V_{\rm MAX}R_{\rm MAX}{}^x = VR^x,$$
 where $x = 1 (= 0.5)$ for the RANK (MRank) model, (2)

$$V = V_{\text{MAX}} \sqrt{\left(\frac{R_{\text{MAX}}}{R}\right)^A e^{1 - \left(\frac{R_{\text{MAX}}}{R}\right)^A}} \text{ (the H80 model) (3)}$$

In Eqs. 2 and 3, R denotes the radius from the center of a TC and V is the surface wind speed at R. Following [55], we consider A = 1.5 in evaluating the performance of the H80 model, within the suggested range (0.75 to 2.5) for the value of A by H80. Note that the main difference between H80 and H10 is that H10 treats the power of the term inside the square root of Eq. 3 as a function of R instead of a constant, which essentially is a continuous piecewise fitting model.

As indicated in panels B and C of Figs. 1, 2, 4, and 5 as well as panel D of Fig. 3, there are no unphysical solutions in the revised Rankine vortex and H80 models. The solutions obtained from these two models are well correlated with their observational counterparts with a correlation skill range of 0.6 to 0.95. The values of MAE for $V_{\rm MAX}$ and $R_{\rm MAX}$ in the modified Rankine vortex model are within their observational resolution, but its

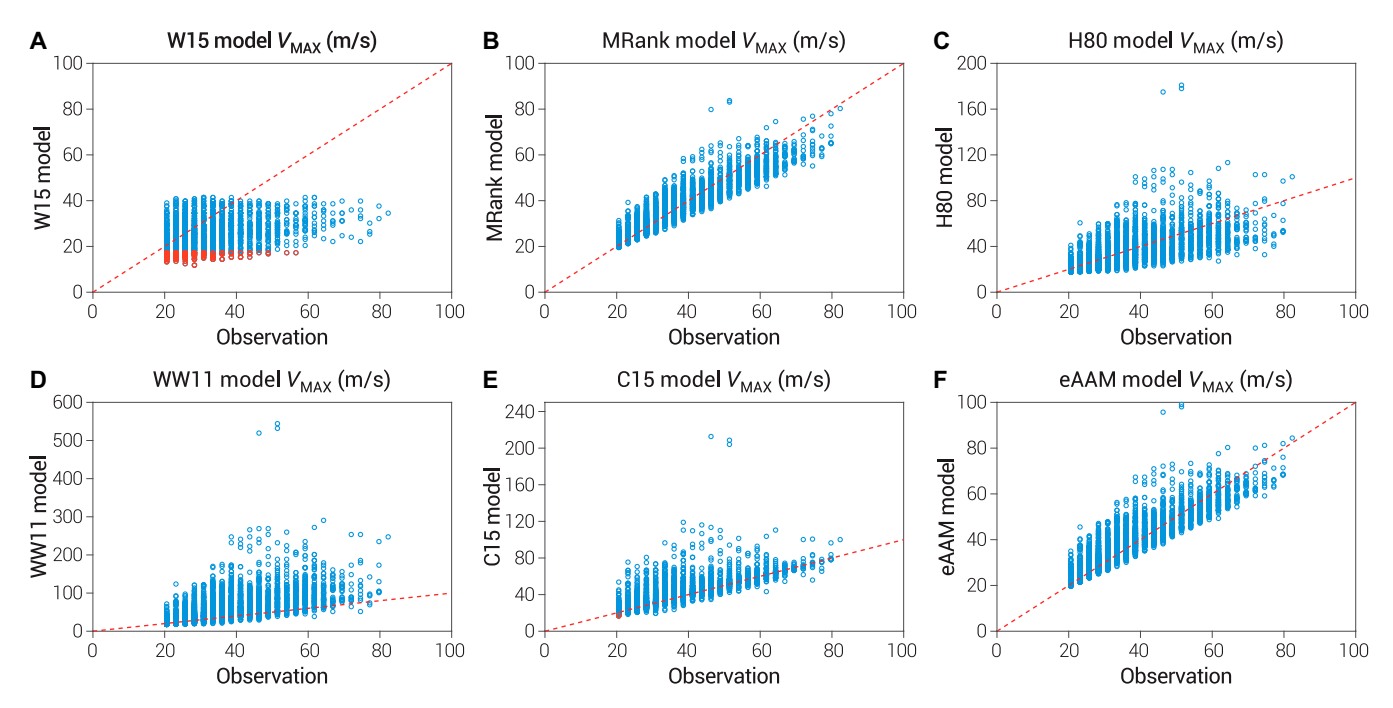


Fig. 1. Scatterplots of model solutions for V_{MAX} (ordinate) against observations (abscissa). (A) W15 model. (B) Modified Rankine vortex model. (C) H80 model. (D) WW11 model. (E) C15 model. (F) eAAM model. Red circles represent the unphysical solutions whose V_{MAX} is less than 17.5 m s⁻¹.

MAE for R_{17} is still large, approximately 4 times (or 40 km) as large as the observational resolution. Nevertheless, the MAE values for $V_{\rm MAX}$, V_{17} , and $R_{\rm MAX}$ of the modified Rankine vortex and H80 models are no greater than 2 times as large as the observational resolution. In particular, their MAE values for V_{17} are less than the observational resolution in winds, and those for $V_{\rm MAX}$ are only modestly greater (approximately 20 to 50%) than the observational resolution in winds. The mean errors (Fig. 3C) in the modified Rankine vortex are smaller

than those of the H80 model. The latter has a negative systematic error in the solution for $V_{\rm MAX}$ and $R_{\rm MAX}$ and a positive systematic error in the solution for $V_{\rm 17}$ and $R_{\rm 17}$ (Fig. 3C). The larger systematic errors of the H80 model than the modified Rankine vortex model are also evident from the more noticeable deviations from the diagonal line in these scatterplots (Figs. 1C, 2C, and 4C) and the noncentered red line in the histogram (Fig. 5C). The systematic underestimation of TC intensity by the H80 model can be reduced substantially by

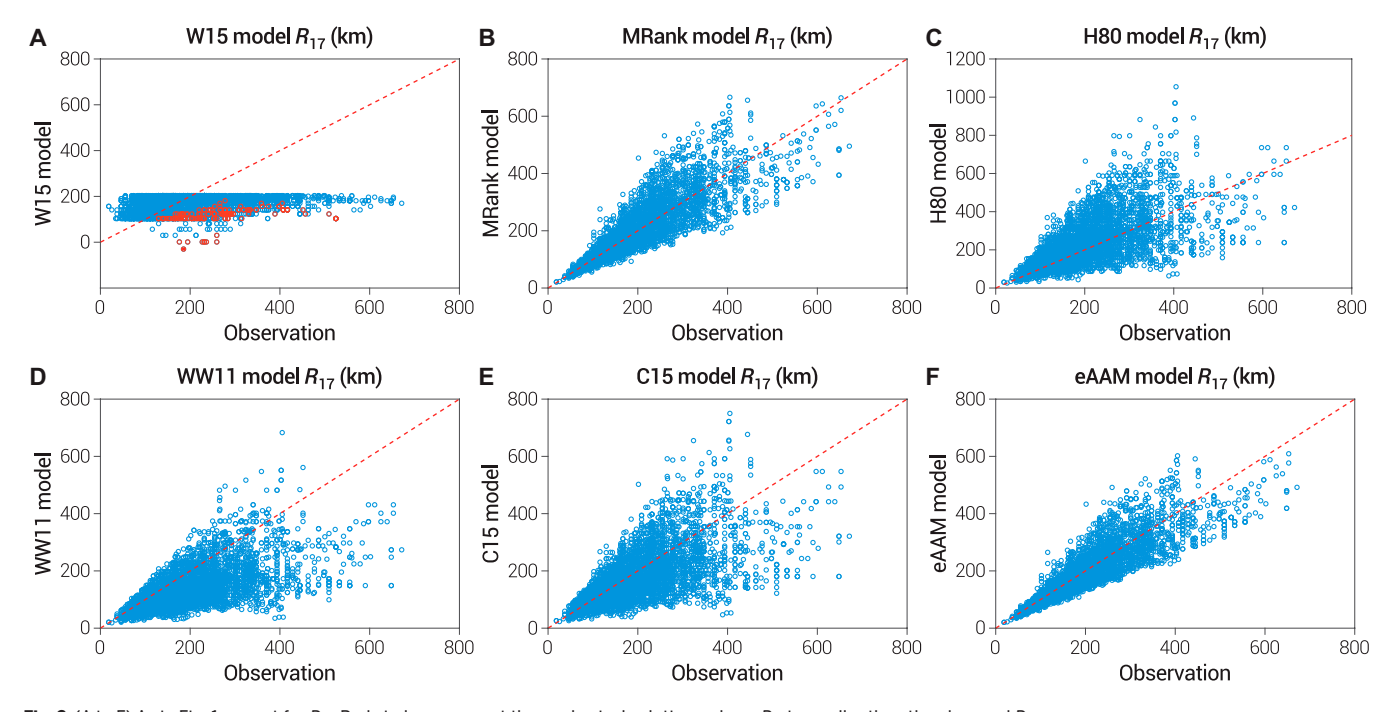


Fig. 2. (A to F) As in Fig. 1, except for R_{17} . Red circles represent the unphysical solutions whose R_{17} is smaller than the observed R_{MAX} .

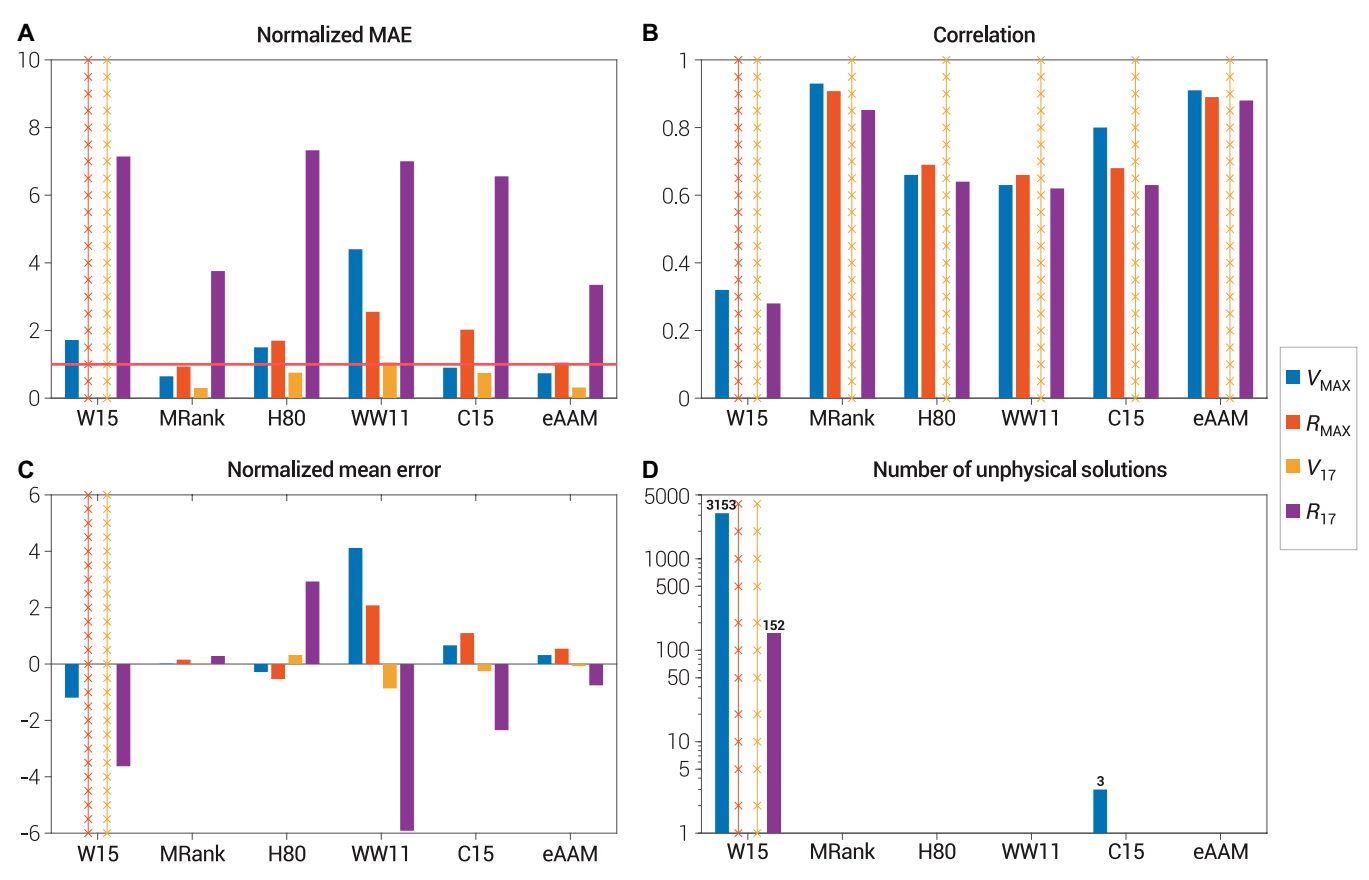


Fig. 3. Bar charts for the performance metrics of (A) MAE (mean absolute errors), (B) Corr (correlation skill), (C) MErr (systematic errors), and (D) the number of unphysical solutions for all the models analyzed in this study (the abscissa). The values of the metrics (ordinate) are evaluated according to their mathematical definitions provided in Table 1, except for MAE and MErr displayed in (A) and (C), in which the original values of MAE and MErr for V_{MAX} and V_{17} are normalized by 5 m s⁻¹, and R_{MAX} and R_{17} , are normalized by 10 km. The red horizontal line at the tick mark of 1.0 in (A) corresponds to the observational resolution in wind (5 m s⁻¹) and radius (10 km). Because the W15 model cannot be used to estimate R_{MAX} and R_{17} , the performance metrics are not applicable, as indicated by vertical lines with "x." Additionally, because the observed V_{17} is a constant (=17.49 m s⁻¹), the correlation skill is not applicable to the solutions for V_{17} . For this reason, there are no data for the correlation skill of the solutions for V_{17} with the observed V_{17} in (B).

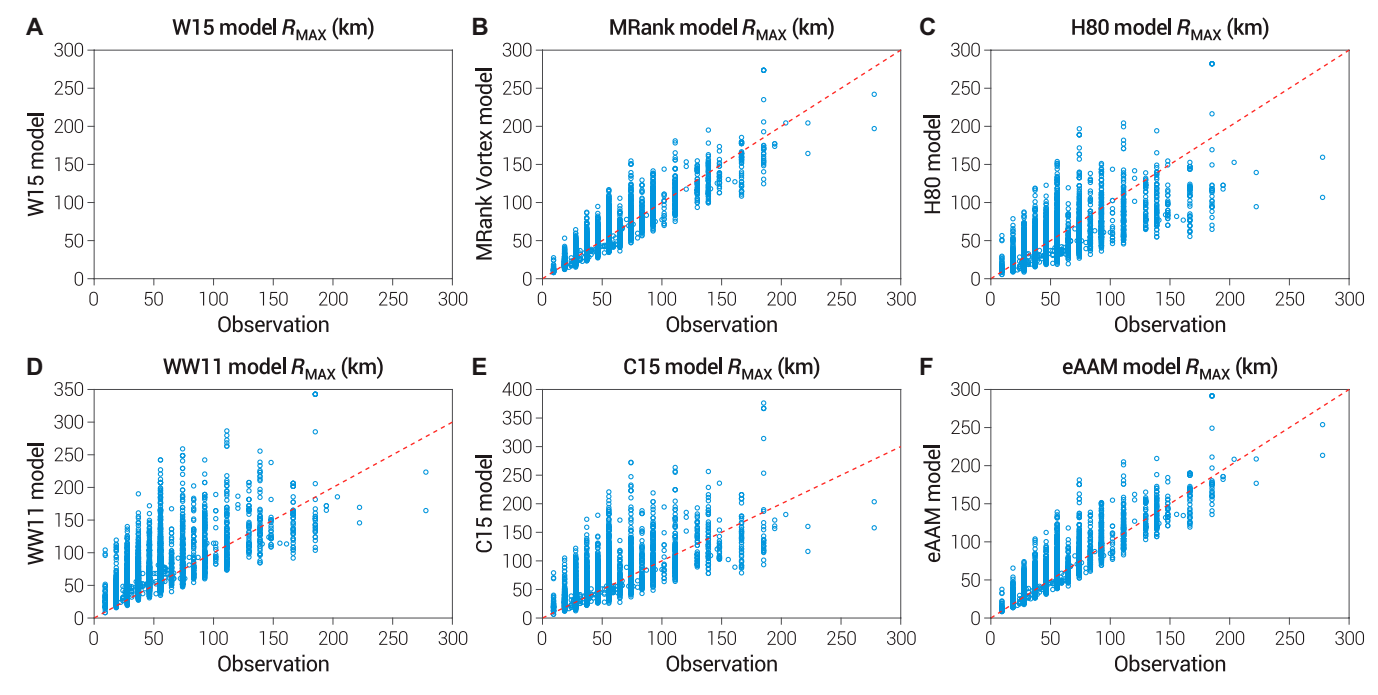


Fig. 4. (A to F) As in Fig. 1 except for R_{MAX} solutions. Note that there are no data points in (A) because the W15 model cannot be used to estimate R_{MAX}

using a larger value of parameter A but at the expense of increasing the MAE value.

Parametric models

We consider the parametric model of Wood and White [39] as being representative of parametric models, which is given by

$$V = V_{\text{MAX}} \frac{\eta^{\lambda} \rho^{\kappa}}{\left(\eta - \kappa + \kappa \rho^{\eta/\lambda}\right)^{\lambda}} \tag{4}$$

where $\rho = R/R_{\text{MAX}}$, $\lambda = 0.5$, $\eta = 2.0$, $\kappa = 1.0$, and the other symbols are the same as their counterparts defined in Eqs. 2 and 3.

Figures 1D, 2D, 4D, and 5D show the direct comparisons of the solutions of the WW11 model against their observational counterparts, whereas the performance metrics of the WW11 model are provided in Fig. 3. In addition to no unphysical solutions, solutions from the WW11 model have correlations of approximately 0.6 to 0.7 that are similar to their counterparts from the idealized models (i.e., MRand and H80 models), as is the MAE for R_{17} , which is approximately 80 km or approximately 8 times larger than the observational resolution in radius. However, the MAE values for V_{MAX} , V_{17} , and R_{MAX} of the WW11 model are noticeably greater than their counterparts of the idealized models. In particular, the MAE value for $V_{\rm MAX}$ of the WW11 model is nearly 4.6 times as large as the observational resolution in winds, or equivalent to an MAE of approximately 23 m s⁻¹. As indicated in Figs. 1D 2D, 3D, and 4D, the large MAE value for $V_{\rm MAX}$ in the WW11 model is caused by the systematic excessive overestimation of $V_{\rm MAX}$, which is accompanied by the systematic overestimation of R_{MAX} , at the expense of the systematic excessive underestimation of V_{17} and R_{17} . The systematic overestimation of $V_{\rm MAX}$ and R_{MAX} and the systematic underestimation of V_{17} and R_{17} (Fig. 3C) are also reflected by pronounced deviations from the diagonal line in these scatterplots for the WW11 model (Figs. 1D, 2D, and 4D) and the noncentered red line in the histogram (Fig. 5D).

Principle-based models

The principle-based models for radial profiles of TC surface winds, including the E04, ER11, and C15 models, are built on the seminal theoretical work of Emanuel [45]. Here, we evaluate the C15 model, as it represents a major improvement to both the E04 and ER11 models by using the ER11 solution over the inner region and the E04 solution over the outer region, which are expressed as

$$\begin{cases} \left(\frac{AAM(R,V)}{AAM(R_{\text{MAX}},V_{\text{MAX}})}\right)^{2-C_k/C_d} = \frac{2(R/R_{\text{MAX}})^2}{2-C_k/C_d\left[1-(R/R_{\text{MAX}})^2\right]}, R_{\text{MAX}} \le R \le R_{\text{merge}} \\ \frac{\partial AAM}{\partial R} = 2\frac{C_d}{W_{\text{cool}}} \frac{RV}{R_0^2 - R^2}, R_{\text{merge}} \le R \le R_0 \end{cases}$$
(5)

where AAM is the absolute angular momentum per unit mass, defined as

$$AAM(R, V) = \frac{1}{2}fR^2 + VR \tag{6}$$

In Eqs. 5 and 6, f is the Coriolis parameter; $C_{\rm k}$ and $C_{\rm d}$ represent the exchange coefficients of enthalpy and momentum in the surface layer, respectively; $W_{\rm cool}$ corresponds to the free tropospheric subsidence in the convective-free outer region; R_0 denotes the radius where surface winds vanish; and $R_{\rm merge}$ is the radius at which the ER11 and E04 solutions intersect. Following C15, we choose $C_{\rm k}=C_{\rm d}=1$ and $W_{\rm cool}=0.002$ to evaluate the C15 model. As in C15, we first solve the two equations in Eq. 5 independently from $R_{\rm MAX}$ to R_0 for each of the

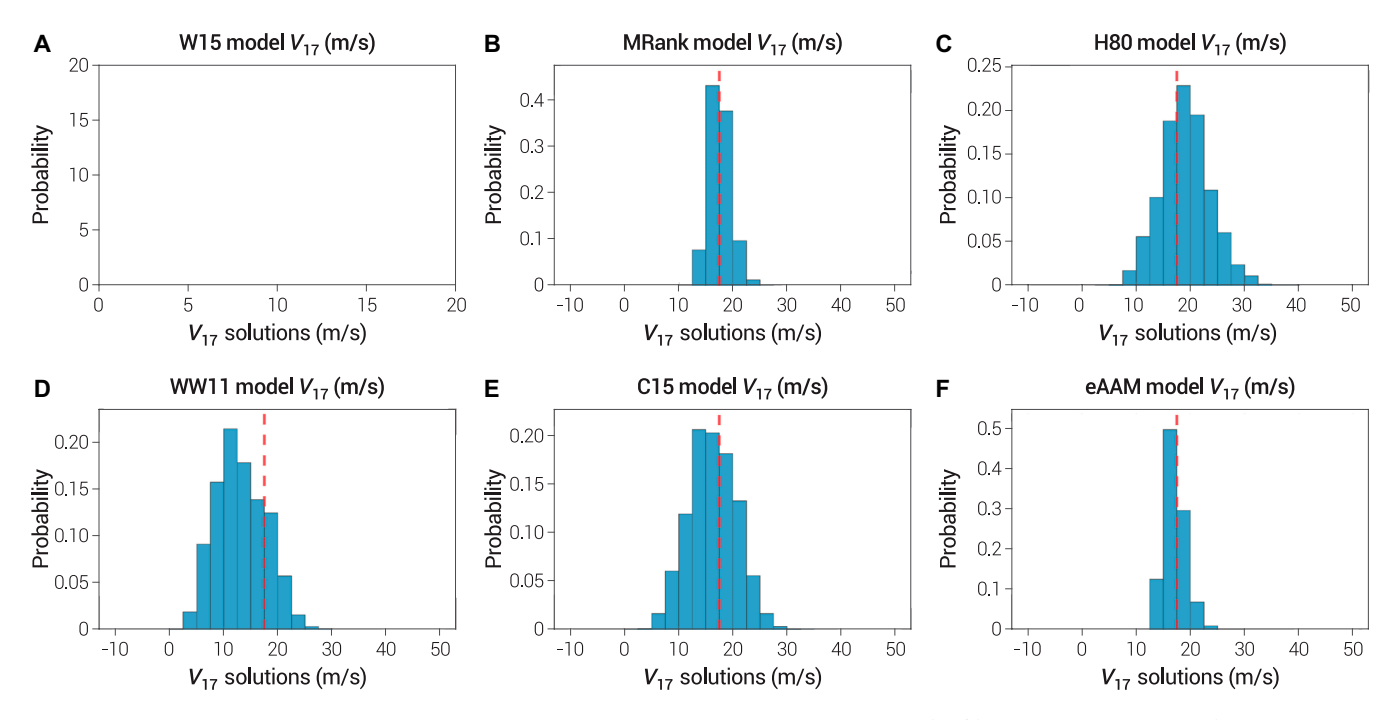


Fig. 5. The histogram (probability distribution) of V_{17} solutions. (A) W15 model. (B) Modified Rankine vortex model. (C) H80 model. (D) WW11 model. (E) C15 model. (F) eAAM model. The dashed red line represents the 17.49 m s⁻¹ wind. Note that there are no data points in (A) because the W15 model cannot be used to estimate V_{17} .

TC records, and then use the ER11 solution for $R_{\text{MAX}} \leq R \leq R_{\text{merge}}$ and the E04 solution for $R \geq R_{\text{merge}}$ as the C15 solution (see Appendix A for details).

Figures 1E, 2E, 4E, and 5E show the direct comparisons of the solutions of the C15 model against their observational counterparts, whereas Fig. 3 provides the performance metrics of the C15 model. The C15 model only has 3 unphysical solutions for $V_{\rm MAX}$, in which $V_{\rm MAX} < V_{17}$. In addition, there are three solutions for $V_{\rm MAX}$, whose values erroneously exceed all reasonable expectations for $V_{\rm MAX}$ (Fig. 1E). Here, we note that the radial profile obtained using the MATLAB codes provided by Chavas [56] always has a peak wind speed equal to the observed $V_{\rm MAX}$. As a result, it is not suitable for finding a solution for $V_{\rm MAX}$ using the observed R_{MAX} in the scenario, in which the radius of the observed $V_{\rm MAX}$ (used as an input to determine the radial profile) is greater than the observed R_{MAX} . We have modified the MATLAB codes for this scenario such that the inwardly constructed radial profile is allowed to increase continuously until the observed $R_{\rm MAX}$ so that the wind speed at the observed R_{MAX} is the solution for V_{MAX} . For very small observed R_{MAX} , this modification may yield excessively large values for V_{MAX} .

In terms of the correlation skill, the solutions obtained from the C15 model have slightly higher correlations with the observations (approximately 0.7 to 0.8) than the H80 and parametric models. Their MAEs for winds are within the observation resolution in wind, but their MAEs for radius are 2 to 7 times as large as the observation resolution in radius. The smallness of the MAE for $V_{\rm MAX}$ of the C15 model is achieved by overestimating $V_{\rm MAX}$ and $R_{\rm MAX}$ and underestimating $V_{\rm 17}$ and $R_{\rm 17}$ (Fig. 3C, or Figs. 1F, 2F, 4F, and 5F). The systematic underestimation of $V_{\rm 17}$ and $R_{\rm 17}$ and the overestimation of $V_{\rm MAX}$ and $R_{\rm MAX}$ suggest that C15 systematically underestimates the loss of AAM.

The eAAM model

The eAAM model described in S22 is built based on the ER11 model. The analysis of 4,984 TC records of the EBTRK dataset reveals that the ER11 model substantially underestimates the inward loss of AAM between R_{17} and $R_{\rm MAX}$. Unlike the ER11 model, in which the inward loss of AAM is only dependent on R, the observed loss of AAM is manifested in terms of the loss of both the RAM (relative angular momentum) and PAM (planetary angular momentum). On the basis of the observational analysis, S22 holistically modified the ER11 model by combining the inward loss terms of RAM and PAM with the AAM term as a radial invariant quantity, referred to as "effective absolute angular momentum" (eAAM), namely,

$$\frac{d(eAAM)}{dR} = 0 (7)$$

where

$$eAAM = \frac{1}{2}fR^2 + VR + \kappa V^{\alpha}R - \frac{1}{2}\lambda fR^{\beta}$$
 (8)

The first two terms on the right-hand side of Eq. 8 are PAM and RAM, respectively, whereas the third and fourth terms represent the inward loss terms of RAM and PAM, respectively. The four parameters α , β , κ , and λ are related to environmental factors in addition to f. Sun et al. [50] show that the four model parameters in Eq. 8 need to satisfy the following conditions:

$$\kappa > 0, \alpha > 1, 1 > \lambda > 0, \text{ and } 2 \ge \beta \ge 1$$
 (9)

to ensure that (a) eAAM is a positive definite quantity, (b) the radial invariant of eAAM always yields an outward decreasing profile of TC tangential wind, (c) AAM always increases with radius monotonically, and (d) the inward loss rates of PAM and RAM are always positive.

We use the default values of the four model parameters, namely, $\alpha = 2.0$, $\beta = 2.0$, $\kappa = 0.22$, and $\lambda = 0.80$, to evaluate the performance of the eAAM. By using constant values of the four parameters, we effectively evaluate the performance of the eAAM model under mean environmental conditions. Figures. 1F, 2F, and 4F, and 5F show the direct comparisons of the solutions of the eAAM model against their observational counterparts. There are no unphysical solutions in the eAAM model. The solutions obtained from the eAAM models have the highest correlations with the observations (approximately 0.8 to 0.95) among all the models under study, i.e., having the lowest MAEs among all of the models. Except for the MAE of R_{17} , which is approximately 3 times as large as the observation resolution for radius, the MAEs for $V_{\rm MAX}$, $V_{\rm 17}$, and $R_{\rm MAX}$ are all less than their corresponding observation resolutions. The small systematic errors (Fig. 3F) indicate that the distributions of the eAAM model's errors for V_{MAX} , V_{17} , R_{MAX} , and R_{17} are all close to a zero-mean distribution, which is also evident from Figs. 1F, 2F, 4F, and 5F. Nevertheless, the systematic underestimation of V_{17} and R_{17} but overestimation of V_{MAX} and R_{MAX} , albeit being the second smallest among all the models under consideration (the modified Rankine vortex model has the smallest systematic errors), suggests that the eAAM model still systematically underestimates the loss of AAM.

It is well known that TC records of the EBTRK dataset have substantial uncertainties, particularly in the records for radii. In Appendix B, we assess the impacts of observational uncertainties in radius on the errors of both the C15 and eAAM models by introducing random perturbations to the 4,984 TC records for both R_{17} and $R_{\rm MAX}$. The range of the random perturbations is between -50% and 50% of their original values in the TC records. The results indicate that the impact of observational uncertainties in radius on errors of the eAAM model is noticeably weaker than that on errors of the C15 model.

Mathematical Characteristics for Enabling a Better Physical Understanding

In this section, we systematically examine whether the models discussed in the "Performance evaluations" section possess the mathematical characteristics listed in Materials and Methods that are deemed necessary to gain a better understanding of the underlying physics governing the observed TC intensity—size relation.

Uniqueness of profiles for winds and radii

Except for the statistical model, the solutions of all the other models for $V_{\rm MAX}$ and V_{17} are obtained from V(R), whereas the solutions for $R_{\rm MAX}$ and R_{17} are obtained from R(V). However, only Rankine vortex models (both original and modified) and the eAAM model are capable of obtaining both $V_{\rm MAX}$ and V_{17} of a TC using the same function V(R) and obtaining both $R_{\rm MAX}$ and R_{17} using the same function R(V) as those mentioned above. As explained in Appendix A, solutions for $V_{\rm MAX}$ of the H80 and C15 (plus E04 and ER11) models are obtained from $V_{\rm inward}(R)$, V_{17} from $V_{\rm outward}(R)$, $R_{\rm MAX}$ from $R_{\rm inward}(V)$, and R_{17}

from $R_{\text{outward}}(V)$. A sufficient condition for a model to satisfy $V_{\text{inward}}(R) = V_{\text{outward}}(R)$ and $R_{\text{inward}}(V) = R_{\text{outward}}(V)$ is

$$\frac{\partial F(R,V)}{\partial R} = 0 \tag{10}$$

where F(R,V) denotes a generic function of R and V. In other words, to satisfy $V(R) = V_{\text{inward}}(R) = V_{\text{outward}}(R)$ and $R(V) = R_{\text{inward}}(V) = R_{\text{outward}}(V)$, the model can be written as a radial invariant quantity, namely, F(R,V) = constant along the radial direction. Furthermore, for models that can be written in the form of Eq. 10, we also have $V(R) = R^{-1}(V)$, or $R(V) = V^{-1}(R)$, where superscript "-1" denotes an inverse function. It follows that the radial profile of a TC constructed from a model would be unique as long as the model can be written as a radial invariant quantity.

Figures 6 to 9 show TC profiles produced by the 6 models under each of the four solution scenarios. These figures are intended mainly for demonstrating which models would have a unique TC profile for the same TC record under the four different solution scenarios. For those models that cannot produce unique TC profiles, one can examine how their TC profiles vary under different solution scenarios. Therefore, our discussions below focus mainly on the general shape of these profiles produced by each model (i.e., comparisons of different panels in the same figure) and under different solution scenarios (i.e., the same panel in different figures), rather than their fine details.

Obviously, the Rankine vortex, modified Rankine vortex, and eAAM models can be written in the general form Eq. 10, but the H80, WW11, and C15 models, as well as the E04 and ER11 models, cannot be written in the general form. A comparison of the profiles shown in Figs. 6C, 7C, 8C, and 9C, which are derived from the H80 model, indicates not only $V_{inward}(R) \neq 0$

 $V_{\text{outward}}(R)$ and $R_{\text{inward}}(V) \neq R_{\text{outward}}(V)$ but also that the inverse of $V_{\text{inward}}(R)$ is not equal to $R_{\text{inward}}(V)$ and the inverse of $V_{\text{outward}}(R)$ is not equal to $R_{\text{outward}}(V)$. One can analytically demonstrate these inequalities for the H80 model by examining the differences between Eqs. A3 and A5. The same can be said for the WW11 model, whose profiles are shown in Figs. 6D, 7D, 8D, and 9D, and outward and inward solutions are given in Eqs. A6 and A8, respectively. For the C15 model (Figs. 6E, 7E, 8E, and 9E), we have $V_{\text{inward}}(R) \neq V_{\text{outward}}(R)$ and $R_{\text{inward}}(V) \neq R_{\text{outward}}(V)$, but the inverse of $V_{\text{inward}}(R)$ is the same as $R_{\text{inward}}(V)$, and the inverse of $V_{\text{outward}}(R)$ is the same as $R_{\text{outward}}(V)$. One can show these inequalities and equalities from the MATLAB codes provided by Chavas [56]. Therefore, the solutions for V_{MAX} , V_{17} , R_{MAX} , and R_{17} of a given TC obtained from the H80 and WW11 models are along 4 different profiles. For the C15 model, the solutions for $V_{\rm MAX}$ and $R_{\rm MAX}$ are obtained along one profile, but the solutions for V_{17} and R_{17} are obtained along a different profile. Therefore, the nonuniqueness of profiles for the same TC record obtained from the H80, WW11, and C15 models makes it nonfeasible to use them to gain a reasonable physical understanding of the TC intensity–size relation.

The profiles shown in Figs. 6B, 7B, 8B, and 9B, which are derived from the modified Rankine vortex model, are identical except for the abscissa and ordinate values at the endpoints. The same can be said for panel F, which is derived from the eAAM model. The differences in the ordinate value at the endpoints are due to the errors of the models' solutions for V_{17} in Fig. 6 against the observed V_{17} and the errors of the models' solutions for V_{MAX} in Fig. 7 against the observed V_{MAX} . Similarly, the differences in the abscissa value at the endpoints are due to the errors of the models' solutions for R_{17} in Fig. 8 against the observed R_{17} and the errors of the models' solutions for R_{MAX}

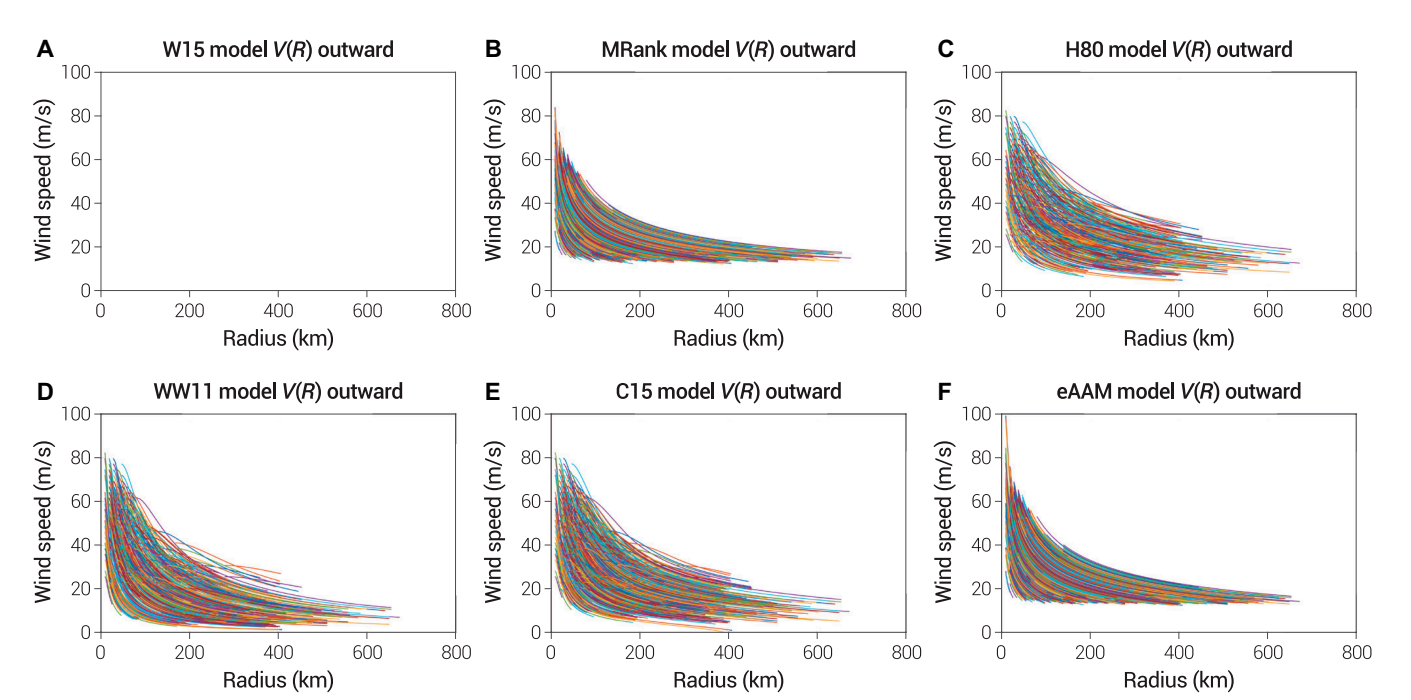


Fig. 6. Outward solutions of winds starting from the observed R_{MAX} and V_{MAX} and ending at the observed R_{17} of the 4,984 TC records for (A) the W15 model, (B) the modified Rankine vortex model, (C) the H80 model, (D) the WW11 model, (E) the C15 model, and (F) the eAAM. The wind profiles are obtained by calculating wind speeds for the radius starting from R_{MAX} until R_{17} . (A) is blank, as the W15 model cannot be used to obtain TC profiles, and it is intentionally retained here to highlight the fact that none of the statistical models can be used to obtain TC profiles, making it infeasible to gain a reasonable physical understanding of the TC intensity–size relation. The colors for the wind profile curves are used to merely differentiate individual TC records of the EBTRK data without any indication of their intensities and sizes.

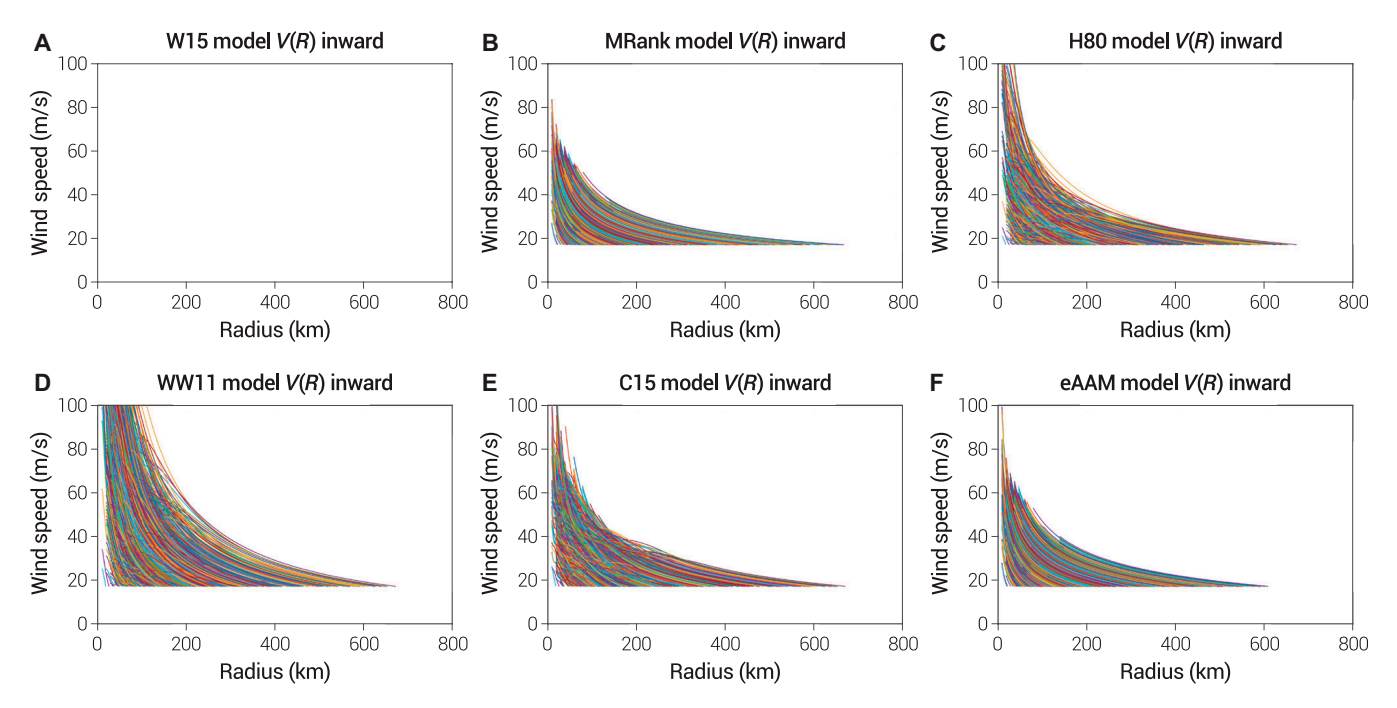


Fig. 7. (A to F) As in Fig. 6 except for the inward solutions of winds starting from the observed R_{17} and V_{17} and ending at the observed R_{MAX} , of the 4,984 TC records. Note that because of the overestimates of V_{MAX} , some of the TC profiles derived from the inward solutions of the H80, WW11, and C15 models exceed the upper limit (100 m s⁻¹) of the ordinate.

in Fig. 9 against the observed $V_{\rm MAX}$. Therefore, the solutions for $V_{\rm MAX}$, V_{17} , $R_{\rm MAX}$, and R_{17} of a given TC obtained from the modified Rankine vortex and eAAM models are along the same profile. Because they are obtained from the same profile, if one of the solutions has errors, the entire profile would not agree with the observations. This finding indicates the presence of errors in the solutions for the remaining three variables. On the other hand, should one of the solutions for $V_{\rm MAX}$, V_{17} , $R_{\rm MAX}$, and R_{17} agree with its observational counterpart, the entire

profile would agree with the observations, including the other three of the four variables (i.e., $V_{\rm MAX}$, V_{17} , $R_{\rm MAX}$, and R_{17}). Because of the uniqueness of their profiles for the same TC record, the Rankine (both original and modified) and eAAM models would meet a minimal requirement that enables them to be used to gain a reasonable physical understanding of the TC intensity–size relation, provided that the errors of their solutions for $V_{\rm MAX}$, V_{17} , $R_{\rm MAX}$, and R_{17} are very close to observational uncertainties. According to the results reported in the

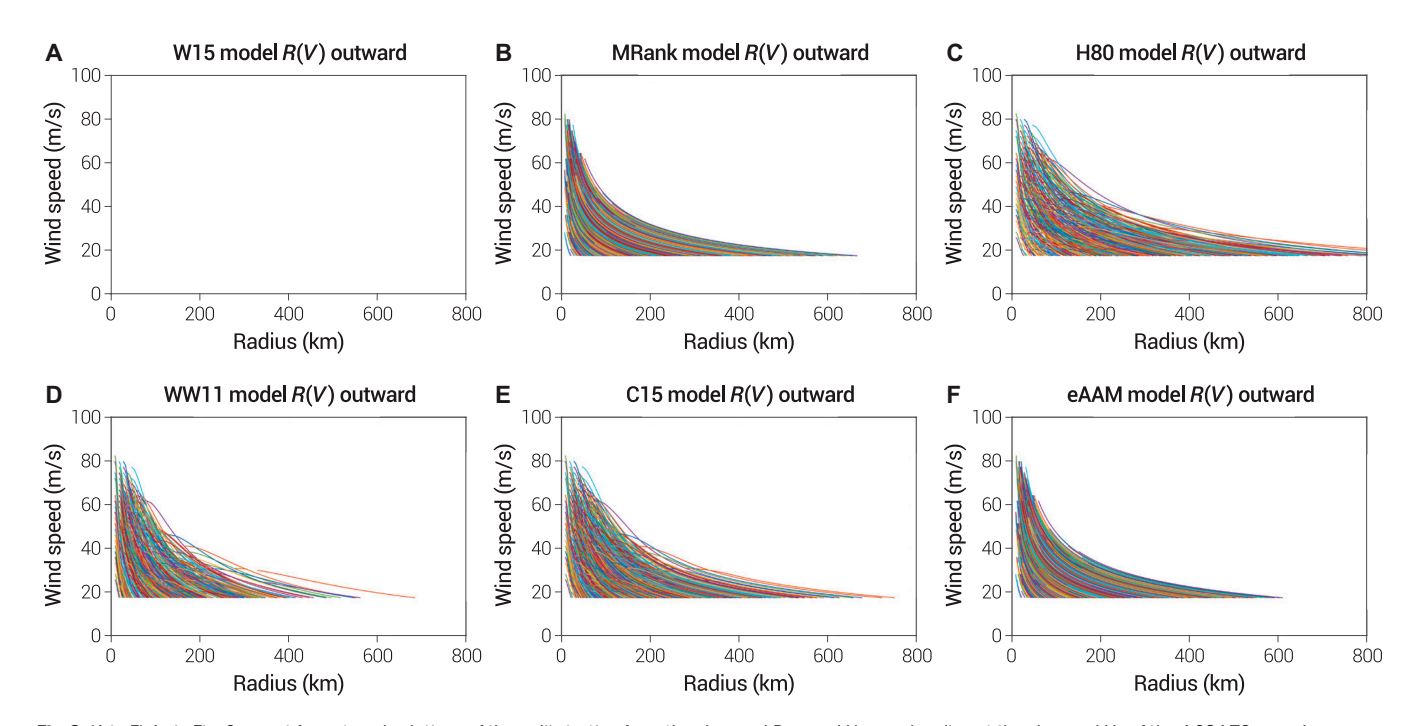


Fig. 8. (A to F) As in Fig. 6 except for outward solutions of the radii starting from the observed R_{MAX} and ending at the observed V_{17} of the 4,984 TC records.

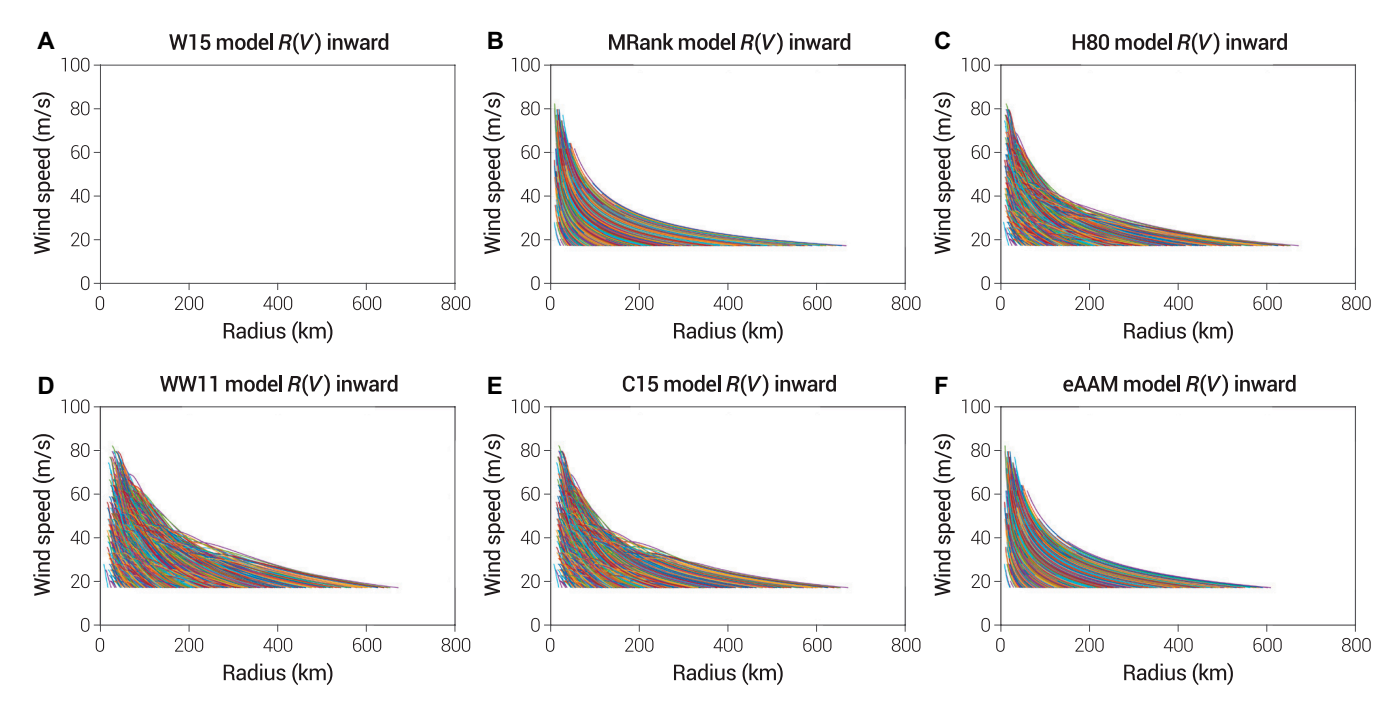


Fig. 9. (A to F) As in Fig. 6 except for inward solutions of radii starting from the observed R₁₇ and V₁₇ and ending at the observed V_{MAX} of the 4,984 TC records.

"Performance evaluations" section, the eAAM model meets the minimal requirement, as the errors of its solutions for $V_{\rm MAX}$, V_{17} , and $R_{\rm MAX}$ are within the observational resolution and the errors of its solutions for R_{17} are close to the observational uncertainties in radius.

In summary, among the six models under study, only the modified Rankine vortex and eAAM models have the same wind profiles for each TC record under the different solution scenarios. Therefore, these two models meet the minimum requirement for reproducing the observed TC profile, namely, the uniqueness of TC profiles for each TC record. The uniqueness of TC profiles is a sufficient and necessary condition that guarantees the accuracy of solutions under all scenarios if the solution obtained under one scenario is accurate. Furthermore, because of the uniqueness of TC profiles, the inaccuracy of the solution obtained under one scenario also implies inaccuracies of the solutions obtained under the other scenarios. In other words, the solution errors of a model meeting the minimum requirement are interrelated, and the error reduction in the solutions for one TC parameter (e.g., V_{MAX}) would automatically guarantee error reduction in the solutions for the other three TC parameters (i.e., V_{17} , R_{17} , and $R_{\rm MAX}$). Specifically, the smallness of systematic errors under one solution scenario also implies the smallness of systematic errors under the other three scenarios, which is the case for the modified Rankine vortex and eAAM models (Fig. 3).

The other three models that are capable of producing TC profiles do not meet the abovementioned minimum requirement. (By design, the W15 model is incapable of producing a TC profile.) As a result, they produce different TC profiles under different solution scenarios for the same TC record. For example, for the H80 model, TC profiles produced by the outward solutions for wind speed (Fig. 6C) tend to decrease with radius much slower than their counterparts by the inward solutions (Fig. 7C), and the outward solutions for radii (Fig. 8C) are much larger than their counterparts of inward solutions

(Fig. 9C). The same conclusion can also be obtained for the WW11 and C15 models.

Finite size of TC profiles

It is evident from Fig. 10 that only the C15 and eAAM models produce profiles with a finite size, namely, the wind profile of a TC ends at a finite radius from the storm center. It is expected from Eq. 2 that the wind fields of the original Rankine and modified Rankine vortex models vanish at $R \rightarrow \infty$ or that the TC profiles predicted by the original Rankine and modified Rankine vortex models cannot have finite sizes. According to Eqs. 3 and 4, the TC profiles predicted by H80 and WW11 also cannot have finite sizes. As pointed out by Zhang et al. [34], because of neglecting the effect of PAM, both the modified Rankine vortex model and the H80 model are not valid over the outer region. A comparison between Fig. 10E and Fig. 10F reveals that for the same TC intensity, the size predicted by the eAAM model is larger than that predicted by the C15 model. This finding is consistent with the fact that the C15 model underestimates the inward loss of AAM because it neglects the loss of the PAM term.

The TC intensity—size relation

It is apparent from Fig. 11 that the observed intensity–size relationship is complex, namely, a large range of different values of $V_{\rm MAX}$ under the same value of R_{17} and a large range of different values of R_{17} for the same value of $V_{\rm MAX}$, although the observed $V_{\rm MAX}$ and R_{17} still exhibit a weak positive correlation for modest-sized TCs whose R_{17} is less than 300 km. Figure 12 shows the counterpart results obtained from the solutions of the models under study. Obviously, the result from the statistical model (W15; Fig. 12A) does not bear any resemblance with the observations. The H80 model solutions (Fig. 12C) tend to superficially favor weak and small TCs whose $V_{\rm MAX}$ is less than 35 m s⁻¹ and R_{17} less than 300 km. The H80 model also tends to

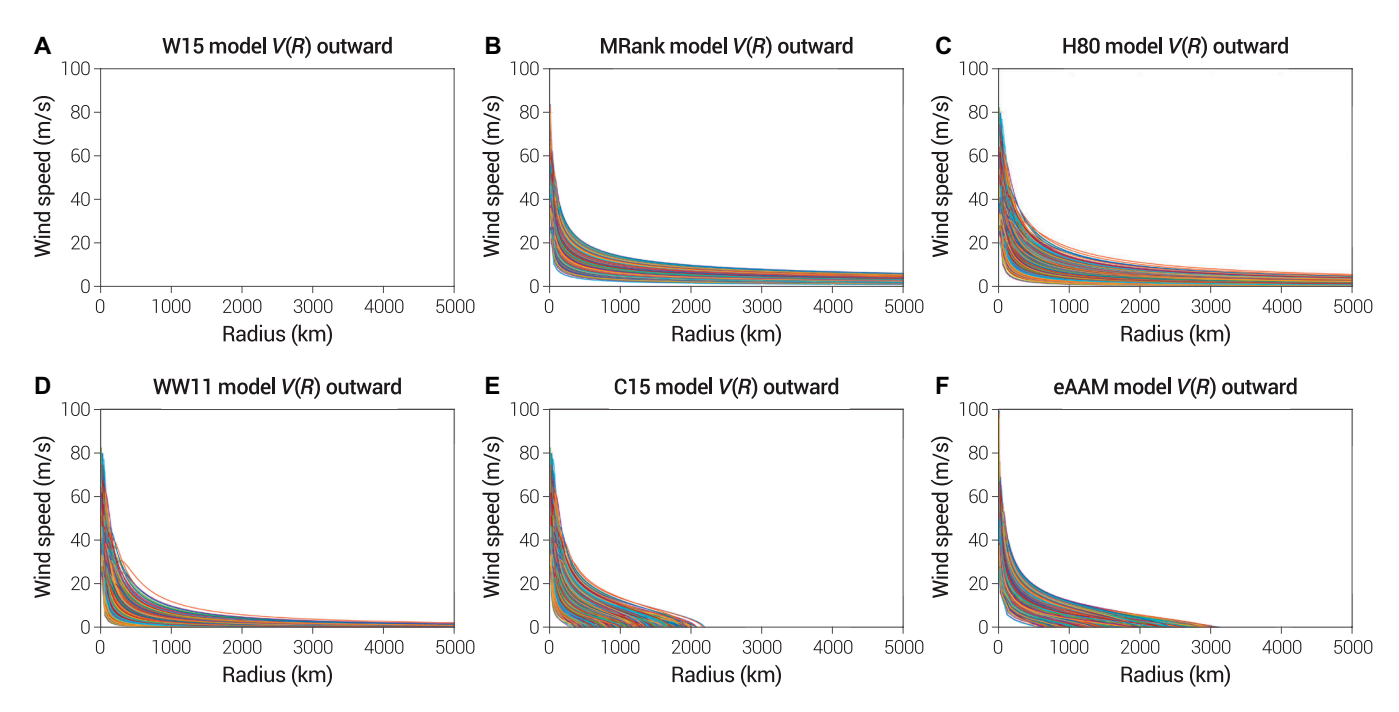


Fig. 10. (A to F) As in Fig. 6, the outward wind solutions are plotted from the R_{MAX} of the 4,984 TC records to 5,000 km.

produce some superficially strong TCs with small sizes and superficially large TCs with weak intensity. The TCs predicted by the parametric model (WW11; Fig. 12D) all tend to be small-sized with R_{17} less than 350 km and tend to be superficially strong with $V_{\rm MAX}$ substantially exceeding the maximum intensity of the observed TCs. The TCs predicted by the modified Rankine vortex (Fig. 12B), C15 (Fig. 12 E), and eAAM (Fig. 12F) models bear a great resemblance with the observations in terms of both the shape and high-density area of the probability density function. As compared to the modified Rankine vortex and eAAM models, the C15 model tends to overestimate TC size, as evidenced by a small but noticeable percentage of its predicted TCs exceeding the observed maximum intensity.

Summary and Concluding Remarks

In this study, we systematically examined the main features and the performance skill of different types of models for TC intensity—size relations against the 4,984 TC records derived from the 6-hourly EBTRK data during 1988 to 2020 [51]. The models under study include the W15 model (a statistical model), modified Rankine vortex and H80 models for idealized TC profile models, the WW11 model for a parametric TC profile model, the C15 model for a principle-based TC profile model, and the eAAM model. Our evaluations are made under at least two implicit assumptions: (a) the observed TC intensity—size relation could be reproduced under the mean environmental conditions, which can be represented by standard constant parameter values of each model, and (b) each of the 4,984 TC records is derived from the azimuthal mean profile of TC surface winds, as all the models under study are for axisymmetric TCs.

There are two types of considerations for evaluating the performance skill of individual models regarding the observed TC records. The first is a set of quantitative metrics that facilitate a direct comparison between the solutions obtained from

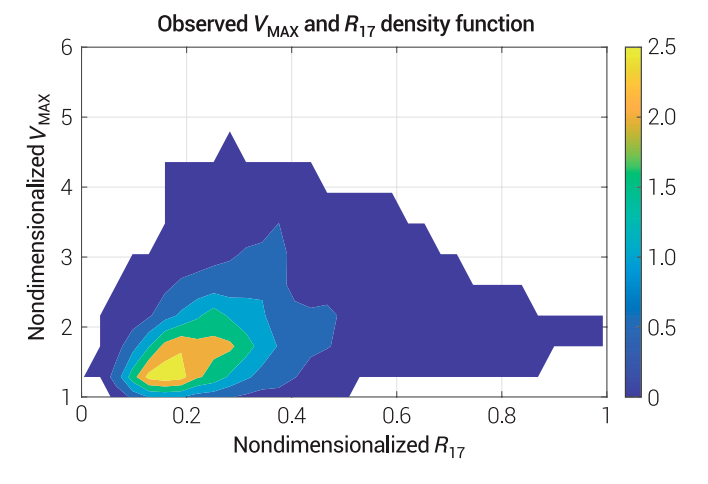


Fig. 11. The probability density function (PDF) as a function of the observed TC intensity (ordinate, V_{MAX} normalized by 17.5 m s⁻¹) and size (abscissa, R_{17} normalized by 670 km corresponding to the largest value of R_{17} among the 4,984 TC records). The PDF is calculated using the Gaussian kernel density estimate algorithm [68].

individual models and the observed TC records. The second type of consideration is a set of mathematical characteristics that are deemed necessary to gain a reasonable understanding of the underlying physics governing the observed TC intensity–size relation.

Table 2 summarizes the main findings of our study. The first row is for a hypothetically perfect model that could be regarded as a "physics law" for the observed TC intensity–size relation because (a) its solutions for $V_{\rm MAX}$, $R_{\rm MAX}$, $V_{\rm 17}$, and $R_{\rm 17}$ are close to their observational counterparts within observational errors; (b) there are no unphysical solutions, namely, that its solutions satisfy $V_{\rm MAX} > V_{\rm 17} > 0$ and $R_{\rm 17} > R_{\rm MAX} > 0$; (c) its solutions for $V_{\rm MAX}$, $R_{\rm MAX}$, $V_{\rm 17}$, and $R_{\rm 17}$ of a given TC are obtained along the

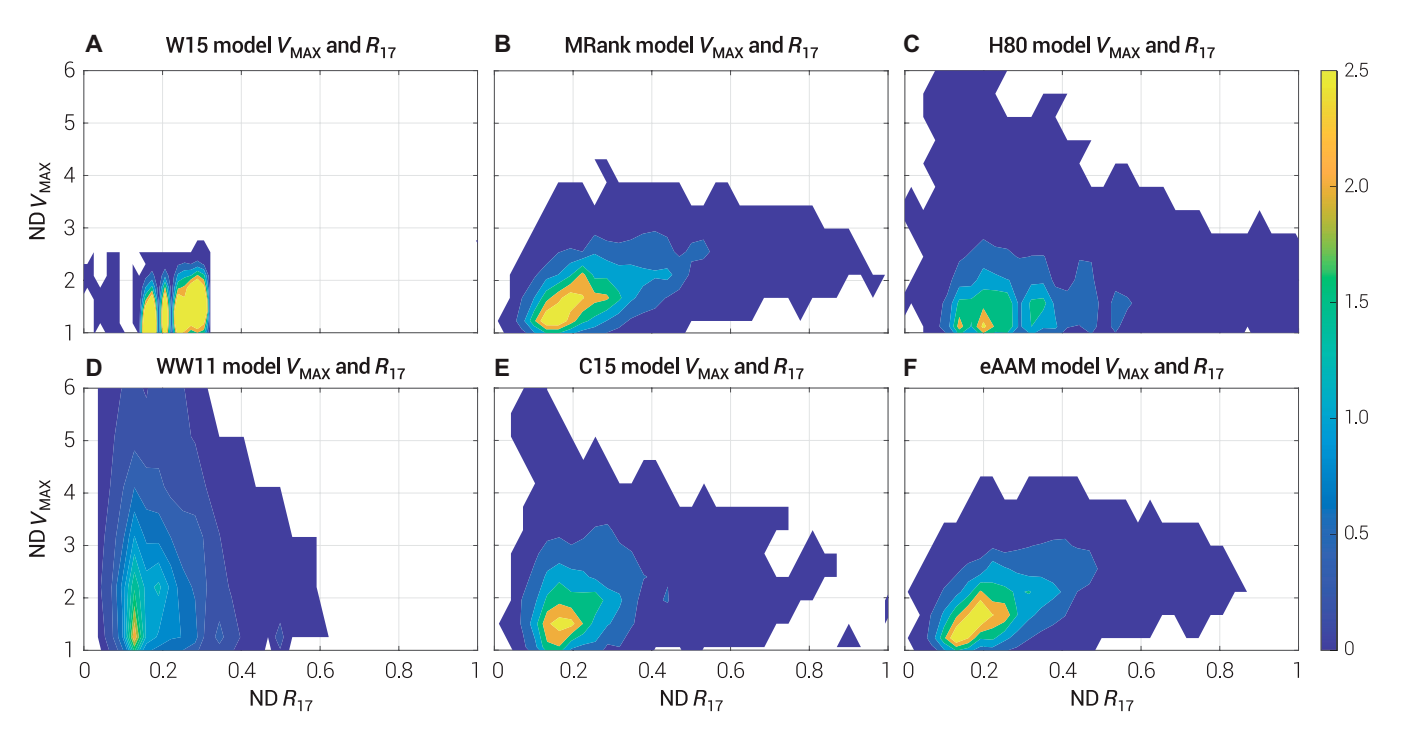


Fig. 12. As in Fig. 11 except for the PDF derived from the solutions of (A) the W15 model, (B) the modified Rankine vortex model, (C) the H80 model, (D) the WW11 model, (E) the C15 model, and (F) the eAAM model. V_{MAX} is calculated using observed R_{MAX} , V_{17} , and R_{17} , while R_{17} is calculated using observed V_{MAX} , and V_{17} . The acronym "ND" stands for "nondimensionalized."

same radial profile of surface winds; and (d) the solutions for surface winds approach zero at a finite radius from the TC center. Conditions (a) to (c) would ensure that the radial profile of the surface winds predicted by the model would overlap with the radial profile of (azimuthal mean) surface winds of an observed TC, provided that one of the solutions for $V_{\rm MAX}$, $R_{\rm MAX}$, $V_{\rm 17}$, and $R_{\rm 17}$ is close to the observed counterpart within observational errors (i.e., the other three solutions would automatically be close to the observed counterparts within observational errors).

According to Table 2, the modified Rankine vortex model behaves comparably to the hypothetically perfect model except that it does not yield finite-sized TC profiles. The modified Rankine vortex model only effectively considers the loss of relative angular momentum by introducing the nonlinear dependency of the regular angular momentum on radius. Because of the effective inclusion of the loss term of planetary angular momentum, radial profiles of surface winds produced by the C15 model are all finite-sized. However, the radial profile of surface wind for a given TC record produced by the C15 model is not unique. The inclusion of the loss of both planetary and relative angular momentum in the eAAM model results in finite-sized TC profiles and further reduces the MAE of the solutions R_{17} obtained by the modified Rankine vortex model. The improvement of the eAAM with respect to the C15 model is achieved by combining the AAM and the loss terms of AAM as a radial invariant quantity, namely, the eAAM. As a result, only the eAAM model is capable of producing a unique finitesized radial profile of surface winds for each TC record, which corresponds to a minimal requirement to ensure that the predicted radial profile of the surface winds would align with the observed profile. In addition to meeting the minimum requirement, the solutions obtained from the eAAM model are well correlated with their observational counterparts (85 to 95%)

with little systematic bias and small absolute mean errors that are very close to the observational resolution. The eAAM model's ability to capture the complex intensity–size relation of observed TCs, in combination with these desirable features, suggests its high potential for gaining a better understanding of the underlying physics governing the observed TC intensity–size relation.

Another unique feature of the eAAM model is its ability to construct the entire radial profile of (azimuthal mean) surface winds using the information at any radius of an observed TC, including the outer regions where TC winds are very weak. As indicated in Table 2, the only other model besides the eAAM model that can do so is the modified Rankine vortex model. However, because the TC profile obtained from the modified Rankine vortex model does not have a finite value of R_0 , it would yield a profile of surface winds whose maximum winds would unrealistically be too strong when using the information over the outer regions. Sun et al. [50] demonstrated the ability of the eAAM model to make real-time assessments of TC winds and size using information over the outer regions where TC surface winds are only a few meters per second; more details can be found at https://amccao.wixsite.com/hurricanewindprofile.

One of our ongoing studies is to further improve the eAAM model by relating the four model parameters to various environmental factors of TCs so that their values can vary under different environmental conditions, such as SST [47], atmospheric relative humidity or the availability of atmospheric moisture [57], vertical wind shear [58], and environmental stratification [59], as well as other internal factors such as domain-mean radial velocity that is related to latent heat release [60,61]. The inclusion of the environmentally dependent model parameters would enhance the eAAM model's ability to predict the temporal evolution of a given TC (e.g., intensification or

Table 2. Summar	y of the performance	e of the TC intensity—size	e models evaluated in this study
-----------------	----------------------	----------------------------	----------------------------------

Model	Mean absolute errors ^a	Unphysical solutions	Uniqueness of wind profiles	Finite R ₀
"Physics laws"	Within observational errors	None	Unique	Finite
W15	$V_{MAX} \sim 9 \text{ m s}^{-1}$; V_{I7} : N/A R_{MAX} : N/A; $R_{I7} \sim 71 \text{ km}$	Many	N/A	N/A
Modified Rankine vortex	$V_{MAX} \sim 3 \text{ m s}^{-1}$; $V_{17} \sim 2 \text{ m s}^{-1}$ $R_{MAX} \sim 9 \text{ km}$; $R_{17} \sim 38 \text{ km}$	None	Unique	Infinite
H80	$V_{MAX} \sim 7 \text{ m s}^{-1}$; $V_{17} \sim 4 \text{ m s}^{-1}$ $R_{MAX} \sim 17 \text{ km}$; $R_{17} \sim 73 \text{ km}$	None	Multiple	Infinite
WW11	$V_{\text{MAX}} \sim 22 \text{ m s}^{-1}; V_{17} \sim 5 \text{ m s}^{-1}$ $R_{\text{MAX}} \sim 26 \text{ km}; R_{17} \sim 70 \text{ km}$	None	Multiple	Infinite
C15	$V_{MAX} \sim 5 \text{ m s}^{-1}$; $V_{17} \sim 4 \text{ m s}^{-1}$ $R_{MAX} \sim 20 \text{ km}$; $R_{17} \sim 66 \text{ km}$	A few	Multiple	Finite
eAAM	$V_{MAX} \sim 4 \text{ m s}^{-1}$; $V_{17} \sim 2 \text{ m s}^{-1}$ $R_{MAX} \sim 10 \text{ km}$; $R_{17} \sim 33 \text{ km}$	None	Unique	Finite

 $^{^{\}mathrm{a}}$ Bold numbers indicate MAEs within the observational resolution, which is 5 m s $^{\mathrm{-1}}$ for winds and 10 km for radii.

weakening) from the temporal changes of its inward loss rates of AAM as well as its eAAM value in response to changes in environmental conditions. In addition, using the environmentally dependent model parameters, one could compare the radial profile of surface wind obtained from the eAAM model to that of an idealized "dry TC" studied by Wang and Lin [62], who demonstrated that the ER11 model can reasonably capture the radial profile of their simulated "dry TC," in which latent heat release is not considered. We believe that the improved eAAM model could then become a potentially powerful tool for helping operational models improve the skill of TC intensity forecasts.

Appendix A Procedures for obtaining solutions to TC intensity—size models

Here, we briefly describe the procedures for obtaining profiles of V(R) and R(V) of the W15, Modified Rankine vortex, H80, WW11, C15, and eAAM models and their solutions for $V_{\rm MAX}$, $R_{\rm MAX}$, $V_{\rm 17}$, and $R_{\rm 17}$ using the observed values of $V_{\rm MAX}$, $R_{\rm MAX}$, $V_{\rm 17}$, and $R_{\rm 17}$.

The W15 model

Equation 1 shows that the W15 model only involves two variables, namely, $V_{\rm MAX}$ and R_{17} . Therefore, the W15 model cannot be used to obtain profiles of V(R) and R(V). To obtain the solution for R_{17} of a TC record, we simply plug in the value of observed $V_{\rm MAX}$ of the TC record into Eq. 1. Similarly, the solution for $V_{\rm MAX}$ of a TC record is obtained by solving Eq. 1 with the corresponding observed R_{17} . Note that there are 2,097 nonreal solutions for $V_{\rm MAX}$ out of the 4,984 TC records due to a negative "delta-term" of the quadratic equation for $V_{\rm MAX}$. Therefore, they are marked as "unphysical solutions" in Fig. 3D.

Rankine vortex model (original and modified)

Both the original and modified Rankine vortex models, as given by Eq. 2, can be rewritten as a radial invariant quantity, namely,

$$\frac{\partial (VR^x)}{\partial R} = 0 \text{ or } VR^x = C \tag{A1}$$

where x = 1 for the original Rankine vortex model and x = 0.5 for the modified Rankine vortex model. For each TC record, we first obtain

$$C = 0.5 [(V_{\text{MAX}})_{\text{obs}} (R_{\text{MAX}})_{\text{obs}}^{x} + (V_{17})_{\text{obs}} (R_{17})_{\text{obs}}^{x}] (A2)$$

Then, we obtain V(R) in the domain of $R \geq (R_{\text{MAX}})_{\text{obs}}$ and R(V) in the domain of $(V_{\text{MAX}})_{\text{obs}} \geq V$ using Eq. A1. As explained in the "Uniqueness of profiles for winds and radii" section, because we write the Rankine (original and modified) vortex models as a radial invariant quantity, the profiles of V(R) in the domain of $(R_{17})_{\text{obs}} \geq R \geq (R_{\text{MAX}})_{\text{obs}}$ and R(V) in the domain of $(V_{\text{MAX}})_{\text{obs}} \geq V \geq (V_{17})_{\text{obs}}$ are identical except at the endpoints of their abscissa and ordinate (see the "Uniqueness of profiles for winds and radii" section for more details). Obviously, surface winds determined from Eq. A1 will not approach zero at a finite value of R. Therefore, we only show V(R) of the Rankine vortex model in the domain of 5,000 km $\geq R \geq (R_{\text{MAX}})_{\text{obs}}$.

The H80 model

By design, the H80 model, as given by Eq. 3, is used to obtain V(R) outwardly from $(V_{\rm MAX})_{\rm obs}$ at $R=(R_{\rm MAX})_{\rm obs}$ to a radius $R>(R_{\rm MAX})_{\rm obs}$. For this reason, we label it $V_{\rm outward}$, namely,

$$V_{\text{outward}} = \left(V_{\text{MAX}}\right)_{\text{obs}} \sqrt{\left(\frac{\left(R_{\text{MAX}}\right)_{\text{obs}}}{R}\right)^{1.5} e^{\left[1 - \left(\frac{\left(R_{\text{MAX}}\right)_{\text{obs}}}{R}\right)^{1.5}\right]}}$$
(A3)

We solve Eq. A3 for $V_{\rm outward}$ as a function of R in the domain of $R_0 > R \ge (R_{\rm MAX})_{\rm obs}$. Because surface winds determined from Eq. A3 will not approach zero at a finite value of R, we set $R_{00} = 5{,}000$ km. The solution of $V_{\rm outward}$ at $R = (R_{17})_{\rm obs}$ obtained from Eq. A3 corresponds to the solution of the H80 model for V_{17} . The profile of $R_{\rm outward}$ as a function of V is obtained by solving Eq. A3 for R in the domain of $V_{\rm MAX} = V_{\rm obs} = V_{\rm obs} = V_{\rm obs}$. The

solution of R_{outward} at $V = (V_{17})_{\text{obs}}$ corresponds to the solution of the H80 model for R_{17} .

There are two options to make the H80 model solvable starting from $(V_{17})_{\rm obs}$ and $(R_{17})_{\rm obs}$ inwardly to $R=(R_{\rm MAX})_{\rm obs}$. The first option is to apply Eq. A3 and obtain $V_{\rm MAX}$ using $(R_{\rm MAX})_{\rm obs}$, namely,

$$V_{\text{MAX}} = V_{17} \left\{ \left(\frac{\left(R_{\text{MAX}} \right)_{\text{obs}}}{\left(R_{17} \right)_{\text{obs}}} \right)^{1.5} e^{\left[1 - \left(\frac{\left(R_{\text{MAX}} \right)_{\text{obs}}}{\left(R_{17} \right)_{\text{obs}}} \right)^{1.5} \right]} \right\}^{-\frac{1}{2}}$$
(A4)

Then, the equation for $V_{\rm inward}$ as a function of R in the domain $(R_{17})_{\rm obs} \ge R \ge (R_{\rm MAX})_{\rm obs}$ can be obtained by substituting $(V_{\rm MAX})_{\rm obs}$ into Eq. A3 with the right-hand side of Eq. A4, i.e.,

 $V_{\text{inward}} =$

$$(V_{17})_{\text{obs}}\sqrt{\left(\frac{(R_{17})_{\text{obs}}}{R}\right)^{1.5}e^{\left[\left(\frac{(R_{\text{MAX}})_{\text{obs}}}{(R_{17})_{\text{obs}}}\right)^{1.5}-\left(\frac{(R_{\text{MAX}})_{\text{obs}}}{R}\right)^{1.5}\right]}}$$
(A5)

We solve Eq. A5, for $V_{\rm inward}$ as a function of R in the domain of $(R_{17})_{\rm obs} \geq R \geq (R_{\rm MAX})_{\rm obs}$. The solution of $V_{\rm inward}$ at $R = (R_{\rm MAX})_{\rm obs}$ obtained from Eq. A4, which is the same as that from Eq. A4, corresponds to the solution of the H80 model for $V_{\rm MAX}$. To obtain the profile of $R_{\rm inward}$ as a function of V, we also first obtain $R_{\rm MAX}$, which corresponds to the solution of H80 for $R_{\rm MAX}$, using Eq. A4 by setting $V_{\rm MAX} = (V_{\rm MAX})_{\rm obs}$. The profile of $R_{\rm inward}$ as a function of V can be obtained by solving Eq. A5 for R in the domain $(V_{\rm MAX})_{\rm obs} \geq V \geq (V_{17})_{\rm obs}$.

The second option is to simply substitute $(V_{\rm MAX})_{\rm obs}$ with $V_{\rm inward}$, R with $(R_{17})_{\rm obs}$, $(R_{\rm MAX})_{\rm obs}$ with R, and $V_{\rm outward}$ with $(V_{17})_{\rm obs}$ in Eq. A3, which yields

$$V_{\text{inward}} = \left(V_{17}\right)_{\text{obs}} \sqrt{\left(\frac{\left(R_{17}\right)_{\text{obs}}}{R}\right)^{1.5} e^{-\left[1 - \left(\frac{\left(R_{\text{MAX}}\right)_{\text{obs}}}{\left(R_{17}\right)_{\text{obs}}}\right)^{1.5}\right]} (A5^*)}$$

Obviously, both Eqs. A5 and A5* have the same value for $V_{\rm inward}$ at $R=(R_{\rm MAX})_{\rm obs}$. The same can be said for the value of $V_{\rm inward}$ at $R=(R_{17})_{\rm obs}$. However, $(R_{17})_{\rm obs}>R>(R_{\rm MAX})_{\rm obs}$, Eqs. A5 and A5* would yield different values of $V_{\rm inward}$, or the profile determined from Eq. A5 would not be the same as that from Eq. A5*, except at $R=(R_{17})_{\rm obs}$ and $R=(R_{\rm MAX})_{\rm obs}$. Because Eq. A5 is more in accordance with the original design of the H80 model, namely, it is used to solve for V(R) outwardly, the results for $V_{\rm inward}$ reported in this study are obtained using Eq. A5.

The WW11 model

Similar to the H80 model, the WW11 model given by Eq. 4 is also designed to obtain V(R) outwardly from $(V_{\rm MAX})_{\rm obs}$ at $R=(R_{\rm MAX})_{\rm obs}$ to a radii $R>(R_{\rm MAX})_{\rm obs}$. For this reason, we label it $V_{\rm outward}$, namely,

$$V_{\rm outward} = \left(V_{\rm MAX}\right)_{\rm obs} \frac{\eta^{\lambda} \left(R/\left(R_{\rm MAX}\right)_{\rm obs}\right)^{\kappa}}{\left[\eta - \kappa + \kappa \left(R/\left(R_{\rm MAX}\right)_{\rm obs}\right)^{\eta/\lambda}\right]^{\lambda}} \, ({\rm A6})$$

where $\lambda=0.5$, $\eta=2.0$, $\kappa=1.0$. We solve Eq. A6 for $V_{\rm outward}$ as a function of R in the domain of $R_0>R\geq (R_{\rm MAX})_{\rm obs}$. Because surface winds determined from Eq. A6 would not approach

zero at a finite value of R, we set $R_0 = 5,000$ km. The solution of $V_{\rm outward}$ at $R = (R_{17})_{\rm obs}$ obtained from Eq. A6 corresponds to the solution of the WW11 model for V_{17} . The profile of $R_{\rm outward}$ as a function of V is obtained by solving Eq. A6 for R in the domain of $(V_{\rm MAX})_{\rm obs} \geq V > 0$. The solution of $R_{\rm outward}$ at $V = (V_{17})_{\rm obs}$ corresponds to the solution of the WW11 model for R_{17} .

There are also two options to make the WW11 model solvable starting from $(V_{17})_{\rm obs}$ and $(R_{17})_{\rm obs}$ inwardly to $R=(R_{\rm MAX})_{\rm obs}$. For the H80 model, we will only consider the option in accordance with the original design of the WW11 model, namely, solving for V(R) outwardly. To do so, we first apply Eq. A6 and obtain $V_{\rm MAX}$ with $(R_{\rm MAX})_{\rm obs}$, i.e.,

$$V_{\text{MAX}} = \left(V_{17}\right)_{\text{obs}} \frac{\left[\eta - \kappa + \kappa \left(\left(R_{17}\right)_{\text{obs}} / \left(R_{\text{MAX}}\right)_{\text{obs}}\right)^{\eta/\lambda}\right]^{\lambda}}{\eta^{\lambda} \left(\left(R_{17}\right)_{\text{obs}} / \left(R_{\text{MAX}}\right)_{\text{obs}}\right)^{\kappa}} (A7)$$

Then, the equation for $V_{\rm inward}$ as a function of R in the domain $(R_{17})_{\rm obs} \ge R \ge (R_{\rm MAX})_{\rm obs}$ can be obtained by substituting $(V_{\rm MAX})_{\rm obs}$ into Eq. A6 with the right-hand side of Eq. A7, which is

 $V_{inward} =$

$$(V_{17})_{\text{obs}} \frac{\left(R/\left(R_{17}\right)_{\text{obs}}\right)^{\kappa} \left[\eta - \kappa + \kappa \left(\left(R_{17}\right)_{\text{obs}}/\left(R_{\text{MAX}}\right)_{\text{obs}}\right)^{\eta/\lambda}\right]^{\lambda}}{\left[\eta - \kappa + \kappa \left(R/\left(R_{\text{MAX}}\right)_{\text{obs}}\right)^{\eta/\lambda}\right]^{\lambda}}$$
(A8)

We solve Eq. A8 for $V_{\rm inward}$ as a function of R in the domain of $(R_{17})_{\rm obs} \geq R \geq (R_{\rm MAX})_{\rm obs}$. The solution of $V_{\rm inward}$ at $R = (R_{\rm MAX})_{\rm obs}$ obtained from Eq. A8, which is exactly the same as that from Eq. A7, corresponds to the solution of the WW11 model for $V_{\rm MAX}$. To obtain the profile of $R_{\rm inward}$ as a function of V, we also first obtain $R_{\rm MAX}$, which corresponds to the solution of WW11 for $R_{\rm MAX}$, using Eq. A7 by setting $V_{\rm MAX} = (V_{\rm MAX})_{\rm obs}$. The profile of $R_{\rm inward}$ as a function of V can be obtained by solving Eq. A8 for R in the domain of $(V_{\rm MAX})_{\rm obs} \geq V \geq (V_{17})_{\rm obs}$.

The C15 model

The C15 model wind profiles are calculated using the MATLAB codes provided by Chavas [56]. Specifically, the value of C_k/C_d is fixed as 1, and the value of $W_{\rm cool}$ is 0.002. The calculations are divided into two groups: (a) an outer-regional profile and solutions for V_{17} and R_{17} and (b) an inner-regional profile and solutions for $V_{\rm MAX}$ and $R_{\rm MAX}$. For (a), the paired values of $(V_{\text{MAX}}, R_{\text{MAX}})$ are taken as input, and the entire wind profile from R_{MAX} to R_0 is automatically generated by the codes given in [56]. Then, the solution for V_{17} can be found as the wind speed at the radius that is closest to the observed R_{17} , and the solution for R_{17} can be found as the radius where the wind speed is closest to the observed wind speed of V_{17} . Unlike the H80 and WW11 models, the outward profiles of V(R) and R(V)of the C15 model are identical except at their endpoints of the observed R_{17} and V_{17} , respectively. For (b), the paired values of (V_{17}, R_{17}) and the value of V_{MAX} (needed by the codes) are taken as input, and the entire wind profile from the calculated $R_{\rm MAX}$ to R_0 is automatically generated by the codes given in [56]. Notably, the original code provided in [56] calculates only R_{MAX} , which is often not the same as the observed R_{MAX} . In the scenario in which the calculated R_{MAX} is less than the observed R_{MAX} , we can directly obtain the solution for V_{MAX} using the value

of V along its inward profile at the observed $R_{\rm MAX}$. In the scenario in which the calculated $R_{\rm MAX}$ is greater than the observed $R_{\rm MAX}$, we have to modify the MATLAB codes such that the inwardly constructed radial profile produced by the original code is allowed to extend continuously until the observed $R_{\rm MAX}$. Following ER11, the extended portion of the inward profile for this scenario is determined by solving the equation given below for V as a function of R from the calculated $R_{\rm MAX}$ to the observed $R_{\rm MAX}$, wherever the calculated $R_{\rm MAX}$ is greater than the observed $R_{\rm MAX}$:

$$\left(\frac{\left(V_{\text{MAX}}\right)_{\text{obs}}\left(R_{\text{MAX}}\right)_{\text{calculated}} + 0.5f\left[\left(R_{\text{MAX}}\right)_{\text{calculated}}\right]^{2}}{VR + 0.5fR^{2}}\right)^{2 - C_{k}/C_{d}} = \frac{2\left(\left(R_{\text{MAX}}\right)_{\text{calculated}}/R_{\text{MAX}}\right)^{2}}{2 - C_{k}/C_{d}\left[1 - \left(\left(R_{\text{MAX}}\right)_{\text{calculated}}/R_{\text{MAX}}\right)^{2}\right]}$$
(A 9)

Similarly, the inward profiles of V(R) and R(V) of the C15 model are also identical except at their endpoints of the observed $R_{\rm MAX}$ and $V_{\rm MAX}$, respectively. However, unlike a model of radiant invariant quantity (e.g., the Rankine vortex mode or the eAAM model), the outward profiles of V(R) and R(V) in C15 are different from the inward profiles of V(R) and R(V).

eAAM model

As indicated by Eqs. 7 and 8, the effective eAAM is a radial invariant quantity. Its solutions can be obtained in the same fashion as the Rankine vortex model. Specifically, for each TC record, we first obtain

$$eAAM_{obs} = 0.25f \left\{ \left[\left(R_{MAX} \right)_{obs} \right]^{2} + \left[\left(R_{17} \right)_{obs} \right]^{2} \right\} + \\ 0.5 \times \left\{ \left(V_{MAX} \right)_{obs} \left(R_{MAX} \right)_{obs} + \left(V_{17} \right)_{obs} \left(R_{17} \right)_{obs} \right\} + \\ 0.5 \times \kappa \left\{ \left[\left(V_{MAX} \right)_{obs} \right]^{\alpha} \left(R_{MAX} \right)_{obs} + \left[\left(V_{17} \right)_{obs} \right]^{\alpha} \left(R_{17} \right)_{obs} \right\} - \\ 0.25 \times \lambda f \left\{ \left[\left(R_{MAX} \right)_{obs} \right]^{\beta} + \left[\left(R_{17} \right)_{obs} \right]^{\beta} \right\}$$
(A10)

Then, we obtain its V(R) continuously as a function of R in the domain of $R_0 \ge R \ge (R_{\text{MAX}})_{\text{obs}}$ and its R(V) continuously as a function of V of the TC record in the domain of $(V_{\text{MAX}})_{\text{obs}} \ge V \ge 0$, using

$$\frac{1}{2}fR^2 + VR + \kappa V^{\alpha}R - \frac{1}{2}\lambda fR^{\beta} = eAAM_{obs}$$
 (A11)

As explained in the "Statistical models" section, the profiles of V(R) in the domain of $(R_{17})_{\rm obs} \geq R \geq (R_{\rm MAX})_{\rm obs}$ and R(V) in the domain of $(V_{\rm MAX})_{\rm obs} \geq V \geq (V_{17})_{\rm obs}$ are identical except at the endpoints of their abscissa and ordinate (see the "Statistical models" section for more details). In the domains of $R_0 \geq R \geq (R_{17})_{\rm obs}$ and $(V_{17})_{\rm obs} \geq V \geq 0$, the two profiles, V(R) and R(V), overlap exactly.

Appendix B Impacts of observational uncertainties on errors of the C15 and eAAM models

TC records of the EBTRK have substantial uncertainties, particularly in the records for radius. Specifically, the amplitude of uncertainties for $V_{\rm MAX}$ is approximately 10.8 knots (~5.6 m s⁻¹), and that for R_{17} is 16.9 n mi (~31.3 km). In addition to the official documentation of the EBTRK dataset (i.e., Demuth et al.

[51]), other studies provide additional information on the uncertainties of the EBTRK dataset, which include Torn and Snyder [63], Landsea and Franklin [64], Sampson et al. [65,66], and Combot et al. [67]. According to these studies, the $V_{\rm MAX}$ uncertainty is in the range of 4 to 6 m s⁻¹, the $R_{\rm MAX}$ uncertainty is in the range of 5 to 20 km, and the R_{17} uncertainty is in the range of 20 to 80 km.

Here, we assess the impacts of observational uncertainties in radius on the errors of both the C15 and eAAM models. To assess the impacts of observational uncertainties in R_{MAX} on errors, we solve the eAAM (or C15) model under the same parameter settings using the 4,984 EBTRK records with the original R_{MAX} (which is supposed to have the largest observational uncertainty) and perturbed R_{MAX} (the other three variables being identical to their EBTRK values). Similarly, to assess the impacts of observational uncertainties in R_{17} on errors, we resolve the eAAM (or C15) model under the same parameter settings using the original R_{17} and perturbed R_{17} with the other three variables being unchanged from their original EBTRK values. The perturbed values of R_{MAX} (R_{17}) are equal to the sum of their original values and uniformly distributed random noises ranging from −50% to +50% of the original values of $R_{\text{MAX}}(R_{17})$. The results are summarized in Tables B1 and B2.

As expected, the presence of such hypothetical errors in R_{MAX} (Table B1) and the MAEs of the solutions for V_{MAX} , $R_{\rm MAX}$, V_{17} , and R_{17} all increase in both the eAAM and C15 models. However, the MAEs of the eAAM model under such a hypothetical situation are more within or closer to the estimated uncertainties of the EBTRK data, except for V_{MAX} in the C15 model, whose MAE is slightly smaller. Similarly, the presence of such hypothetical errors in R_{17} and the MAEs of the solutions for V_{MAX} , R_{MAX} , V_{17} , and R_{17} all increase in both the eAAM and C15 models. However, the MAEs of the eAAM model under such a hypothetical situation are more within the estimated uncertainties of the EBTRK data than those of the C15 model. It is also of interest to point out that the sensitivity of the eAAM performance to the noises in R_{17} is less than that to the noises in R_{MAX} , but there is little difference between the sensitivity of the C15 performance to the noises in R_{17} and that to the noises in R_{MAX} .

Table B1. The mean absolute errors (MAEs) of the C15 and eAAM models using the original and randomly perturbed values of $R_{\rm MAX}$

Models/ variables	$V_{\rm MAX}$ (m s ⁻¹)	R _{MAX} (km)	$V_{17} (\text{m s}^{-1})$	R ₁₇ (km)
eAAM	3.7	10.5	1.6	33.5
eAAM with perturbed R_{MAX}	4.8	12.7	2.0	40.0
C15	4.5	20.2	3.7	60.1
C15 with perturbed $R_{ m MAX}$	6.9	24.6	4.7	74.1

Table B2. The mean absolute errors (MAEs) of the C15 and eAAM models using the original and randomly perturbed values of $R_{\rm 17}$

Models/ variables	$V_{\rm MAX}$ (m s ⁻¹)	$R_{\rm MAX}$ (km)	$V_{17} (\text{m s}^{-1})$	R ₁₇ (km)
eAAM	3.7	10.5	1.6	33.5
eAAM with perturbed R_{17}	4.4	12.8	2.0	40.5
C15	4.5	20.2	3.7	60.1
C15 with perturbed R_{17}	6.2	25.3	4.7	74.7

Acknowledgments

Funding: This research was in part supported by grants from the National Science Foundation (AGS-2012479, AGS-2202875, and AGS-2202766) and Climate Program Office of National Oceanic and Atmospheric Administration (NA20OAR4310380). **Author contributions:** M.C. conceived the idea. M.C., D.-L.Z., and G.L. designed the paper structure. J.S. conducted the calculation and visualization. All authors contributed equally to the writing of the manuscript.

Competing interests: The authors declare that they have no competing interests.

Data Availability

All data used in this study are publicly available: The EBTRK can be downloaded from https://rammb2.cira.colostate.edu/research/tropical-cyclones/tc_extended_best_track_dataset/.

References

- 1. Holland G J, Done J M, Douglas R, Saville GR, Ge M. Global tropical cyclone damage potential. In: Collins J, Walsh K, editors. *Hurricane Risk*. Cham: Springer; 2019. p. 23–42.
- Carrasco CA, Landsea CW, Lin YL. The influence of tropical cyclone size on its intensification. Weather Forecast. 2014;29(3):582–590.
- 3. Chan KTF, Chan JCL. Impacts of initial vortex size and planetary vorticity on tropical cyclone size. *Q J R Meteorol Soc.* 2014;140(684):2235–2248.
- 4. Xu J, Wang Y. A statistical analysis on the dependence of tropical cyclone intensification rate on the storm intensity and size in the North Atlantic. *Weather Forecast*. 2015;30:692–701.
- 5. Xu J, Wang Y. Dependence of tropical cyclone intensification rate on sea surface temperature, storm intensity, and size in the western North Pacific. *Weather Forecast*. 2018;33(3):523–537.
- Guo X, Tan ZM. Tropical cyclone fullness: A new concept for interpreting storm intensity. *Geophys Res Lett*. 2017;44(9):4324–4331.

- 7. Guo X, Tan Z-M. Tropical cyclone intensification and fullness: The role of storm size configuration. *Geophys Res Lett*. 2022;49(16):e2022GL098449.
- Song J, Duan Y, Klotzbach PJ. Revisiting the relationship between tropical cyclone size and intensity over the western North Pacific. *Geophys Res Lett.* 2020;47(13):e2020GL088217.
- 9. Rappaport EN, Franklin JL, Avila LA, Baig SR, Beven JL, Blake ES, Burr CA, Jiing JG, Juckins CA, Knabb RD, et al. Advances and challenges at the National Hurricane Center. *Weather Forecast*. 2009;24(2):395–419.
- 10. Cangialosi JP, Blake E, DeMaria M, Penny A, Latto A, Rappaport E, Tallapragada V. Recent progress in tropical cyclone intensity forecasting at the National Hurricane Center. *Weather Forecast.* 2020;35(5):1913–1922.
- 11. Merrill RT. A comparison of large and small tropical cyclones. *Mon Weather Rev.* 1984;112(7):1408–1418.
- 12. Knaff JA, Longmore SP, Molenar DA. An objective satellite-based tropical cyclone size climatology. *J Clim*. 2014;27(1):455–476.
- 13. Knaff JA, Slocum CJ, Musgrave KD, Sampson CR, Strahl BR. Using routinely available information to estimate tropical cyclone wind structure. *Mon Weather Rev.* 2016;144(4): 1233–1247.
- Chan KTF, Chan JCL. Size and strength of tropical cyclones as inferred from QuikSCAT data. *Mon Weather Rev*. 2012;140(3):811–824.
- Liu KS, Chan JCL. Synoptic flow patterns associated with small and large tropical cyclones over the western North Pacific. *Mon Weather Rev.* 2002;130(8):2134–2142.
- 16. Lee CS, Cheung KK, Fang WT, Elsberry RL. Initial maintenance of tropical cyclone size in the western North Pacific. *Mon Weather Rev.* 2010;138(8):3207–3223.
- 17. Chan KTF, Chan JCL. Angular momentum transports and synoptic flow patterns associated with tropical cyclone size change. *Mon Weather Rev.* 2013;141(11):3985–4007.
- Chan KTF, Chan JCL. The outer-core wind structure of tropical cyclones. *J Meteorol Soc Japan. Ser.* 2018;96(4): 297–315.
- Chavas DR, Emanuel KA. A QuikSCAT climatology of tropical cyclone size. *Geophys Res Lett.* 2010;37(18):044558.
- Wu L, Tian W, Liu Q, Cao J, Knaff JA. Implications of the observed relationship between tropical cyclone size and intensity over the western North Pacific. *J Clim*. 2015;28(24):9501–9506.
- 21. Song J, Klotzbach PJ. Wind structure discrepancies between two best track datasets for western North Pacific tropical cyclones. *Mon Weather Rev.* 2016;144(12):4533–4551.
- Chen K, Chen G, Rao C, Wang Z. Relationship of tropical cyclone size change rate with size and intensity over the western North Pacific. *Atmos Oceanic Sci Lett.* 2021;14: Article 100040.
- 23. Chen K, Chen G, Shi D. Reexamination of the relationship between tropical cyclone size and intensity over the Western North Pacific. *Adv Atmos Sci.* 2022;39:1956–1968.
- 24. Wu Q, Ruan Z. Rapid contraction of the radius of maximum tangential wind and rapid intensification of a tropical cyclone. *J Geophys Res Atmos*. 2021;126(3):e2020JD033681.
- Ruan Z, Wu Q. Relationship between size and intensity in North Atlantic tropical cyclones with steady radii of maximum wind. *Geophys Res Lett.* 2022;49(3):e2021GL095632.
- 26. Rankine WJM. *A manual of applied physics*. 10th ed. London: Charles Griff and Co.; 1982. p. 663.

- 27. Deppermann CE. Notes on the origin and structure of Philippine typhoons. *Bull Am Meteorol Soc.* 1947;28(9):399–404.
- 28. Riehl H. Tropical meteorology. New York: McGraw-Hill; 1954. p. 392.
- Riehl H. Some relations between wind and thermal structure of steady state hurricanes. *J Atmos Sci.* 1963;20(4):276–287.
- 30. Chan JC, Williams RT. Analytical and numerical studies of the beta-effect in tropical cyclone motion. Part I: Zero mean flow. *J Atmos Sci.* 1987;44(9):1257–1265.
- 31. DeMaria M. Tropical cyclone track prediction with a barotropic spectral model. *Mon Weather Rev.* 1987;115(10):2346–2357.
- 32. Holland GJ. An analytic model of the wind and pressure profiles in hurricanes. *Mon Weather Rev.* 1980;108(8): 1212–1218.
- Holland GJ, Belanger JI, Fritz A. A revised model for radial profiles of hurricane winds. Mon Weather Rev. 2010;138(12):4393–4401.
- 34. Zhang D-L, Liu Y, Yau MK. A multiscale numerical study of Hurricane Andrew (1992). Part IV: Unbalanced flows. *Mon Weather Rev.* 2001;129(1):92–107.
- Wood VT. A technique for detecting a tropical cyclone center using a Doppler radar. *J Atmos Ocean Technol*. 1994;11(5):1207–1216.
- 36. Willoughby HE, Darling RWR, Rahn ME. Parametric representation of the primary hurricane vortex. Part II: A new family of sectionally continuous profiles. *Mon Weather Rev.* 2006;134(4):1102–1120.
- Wood VT, White LW, Willoughby HE, Jorgensen DP. A new parametric tropical cyclone tangential wind profile model. *Mon Weather Rev.* 2013;141(6):1884–1909.
- Xu Q, Jiang Y, Liu L. Fitting parametric vortices to aliased Doppler velocities scanned from hurricanes. *Mon Weather Rev.* 2014;142(1):94–106.
- 39. Wood VT, White LW. A new parametric model of vortex tangential-wind profiles: Development, testing, and verification. *J Atmos Sci.* 2011;68(5):990–1006.
- Wang S, Toumi R, Czaja A, Kan AV. An analytic model of tropical cyclone wind profiles. Q J R Meteorol Soc. 2015;141:3018–3029.
- Li TH, Wang Y. The role of boundary layer dynamics in tropical cyclone intensification. Part II: Sensitivity to initial vortex structure. J Meteorol Soc Japan Ser. 2021;99(693):555–573.
- Klotzbach PJ, Chan JC, Fitzpatrick PJ, Frank WM, Landsea CW, McBride JL. The science of William M. Gray: His contributions to the knowledge of tropical meteorology and tropical cyclones. *Bull Am Meteorol Soc.* 2017;98(11):2311–2336.
- Kim YC, Matsui M. Analytical and empirical models of tornado vortices: A comparative study. J Wind Eng Ind Aerodyn. 2017;171:230–247.
- 44. Wood VT, Tanamachi RL, White LW. Influences of larger-scale vortex variability on tornado pressure minima in an outer-flow region: Explorations using a parametric tangential wind model. *Mon Weather Rev.* 2017;145(5):1597–1614.
- 45. Emanuel KA. An air-sea interaction theory for tropical cyclones. Part I: Steady-state maintenance. *J Atmos Sci.* 1986;43(6):585–605.
- 46. Emanuel KA. Tropical cyclone energetics and structure. In: Fedorovich E, Rotunno R, Stevens S, editors. *Atmospheric turbulence and mesoscale meteorology*. London: Cambridge University Press; 2004. p. 165–192.
- 47. Emanuel KA, Rotunno R. Self-stratification of tropical cyclone outflow. Part I: Implications for storm structure. *J Atmos Sci.* 2011;68(10):2236–2249.

- 48. Chavas DR, Lin N, Emanuel KA. A model for the complete radial structure of the tropical cyclone wind field. Part I: Comparison with observed structure. *J Atmos Sci.* 2015;72(9):3647–3662.
- Cronin TW. An analytic model for tropical cyclone outer winds. Geophys Res Lett. 2023;50:e2023GL103942.
- 50. Sun J, Cai M, Liu G, Yan R, Zhang D-L. Uncovering the intrinsic intensity–size relationship of tropical cyclones. *J Atmos Sci.* 2022;79(11):2881–2900.
- 51. Demuth JL, DeMaria M, Knaff JA. Improvement of advanced microwave sounding unit tropical cyclone intensity and size estimation algorithms. *J Appl Meteorol Climatol*. 2006;45(11):1573–1581.
- DeMaria M, Knaff JA, Knabb R, Lauer C, Sampson CR, DeMaria RT. A new method for estimating tropical cyclone wind speed probabilities. Weather Forecast. 2009;24:1573–1591.
- 53. Bryan GH, Fritsch JM. 2002: A benchmark simulation for moist nonhydrostatic numerical model. *Mon Weather Rev.* 2002;130:2917–2928.
- 54. Knaff JA, DeMaria M, Molenar DA, Sampson CR, Seybold MG. An automated, objective, multiple-satellite-platform tropical cyclone surface wind analysis. *J Appl Meteorol Climatol*. 2011;50:2149–2166.
- 55. Emanuel KA. The dependence of hurricane intensity on climate. *Nature*. 1987;326:483–485.
- Chavas DR. Code for tropical cyclone wind profile model of Chavas et al (2015, JAS). Purdue University Research Repository; 2022.
- Hill KA, Lackmann GM. Influence of environmental humidity on tropical cyclone size. Mon Weather Rev. 2009;137:3294–3315.
- 58. Wang Y, Holland GJ. Tropical cyclone motion and evolution in vertical shear. *J Atmos Sci.* 1996;53:3313–3332.
- Kieu C, Zhang D-L. The control of environmental stratification on the hurricane maximum potential intensity. *Geophys Res Lett.* 2018;45:6272–6280.
- 60. Zhang DL, Liu Y, Yau MK. A multiscale numerical study of Hurricane Andrew (1992). Part V: Inner-core thermodynamics. *Mon Weather Rev.* 2002(130):2745–2763.
- 61. Wang Y. How do outer spiral rainbands affect tropical cyclone structure and intensity? *J Atmos Sci.* 2009;66:1250–1273.
- 62. Wang D, Lin Y. Size and structure of dry and moist reversible tropical cyclones. *J Atmos Sci.* 2020;77:2091–2114.
- 63. Torn RD, Snyder C. Uncertainty of tropical cyclone best-track information. *Weather Forecast*. 2012;27:715–729.
- 64. Landsea CW, Franklin JL. Atlantic hurricane database uncertainty and presentation of a new database format. *Mon Weather Rev.* 2013;141:3576–3592.
- Sampson CR, Fukada EM, Knaff JA, Strahl BR, Brennan MJ, Marchok T. Tropical cyclone gale wind radii estimates for the western North Pacific. Weather Forecast. 2017;32: 1029–1040.
- Sampson CR, Goerss JS, Knaff JA, Strahl BR, Fukada EM, Serra EA. Tropical cyclone gale wind radii estimates, forecasts and error forecast for the western North Pacific. Weather Forecast. 2018;33:1081–1092.
- 67. Combot C, Mouche A, Knaff JA, Zhao Y, Zhao Y, Vinour L, Quilfen Y, Chapron B. Extensive high-resolution synthetic aperture radar (SAR) data analysis of tropical cyclones: Comparisons with SFMR flights and best track. *Mon Weather Rev.* 2020;148:4545–4563.
- 68. Botev ZI, Grotowski JF, Kroese DP. Kernel density estimation via diffusion. *Ann Stat.* 2010;38:2916–2957.